LETTER

https://doi.org/10.1038/s41586-018-0257-1

# Parasitic helminths induce fetal-like reversion in the intestinal stem cell niche

Ysbrand M. Nusse[1,2,6], Adam K. Savage[3,6], Pauline Marangoni[2], Axel K. M. Rosendahl-Huber[2], Tyler A. Landman[2], Frederic J. de Sauvage[4], Richard M. Locksley[3]* & Ophir D. Klein[2,5]*

**Epithelial surfaces form critical barriers to the outside world and are continuously renewed by adult stem cells[1]. Whereas dynamics of epithelial stem cells during homeostasis are increasingly well understood, how stem cells are redirected from a tissue-maintenance program to initiate repair after injury remains unclear. Here we examined infection by *Heligmosomoides polygyrus*, a co-evolved pathosymbiont of mice, to assess the epithelial response to disruption of the mucosal barrier. *H. polygyrus* disrupts tissue integrity by penetrating the duodenal mucosa, where it develops while surrounded by a multicellular granulomatous infiltrate[2]. Crypts overlying larvae-associated granulomas did not express intestinal stem cell markers, including *Lgr5*[3], in spite of continued epithelial proliferation. Granuloma-associated Lgr5$^-$ crypt epithelium activated an interferon-gamma (IFN-γ)-dependent transcriptional program, highlighted by Sca-1 expression, and IFN-γ-producing immune cells were found in granulomas. A similar epithelial response accompanied systemic activation of immune cells, intestinal irradiation, or ablation of Lgr5$^+$ intestinal stem cells. When cultured in vitro, granuloma-associated crypt cells formed spheroids similar to those formed by fetal epithelium, and a sub-population of *H. polygyrus*-induced cells activated a fetal-like transcriptional program, demonstrating that adult intestinal tissues can repurpose aspects of fetal development. Therefore, re-initiation of the developmental program represents a fundamental mechanism by which the intestinal crypt can remodel itself to sustain function after injury.**

To study how intestinal crypts respond to tissue disruption, we infected *Lgr5*$^{DTRGFP/+}$ (Lgr5–GFP) reporter mice[4] with *H. polygyrus*. Six days after infection, larvae resided within the intestinal wall, and were surrounded by an immune infiltrate. Crypts overlying granulomas

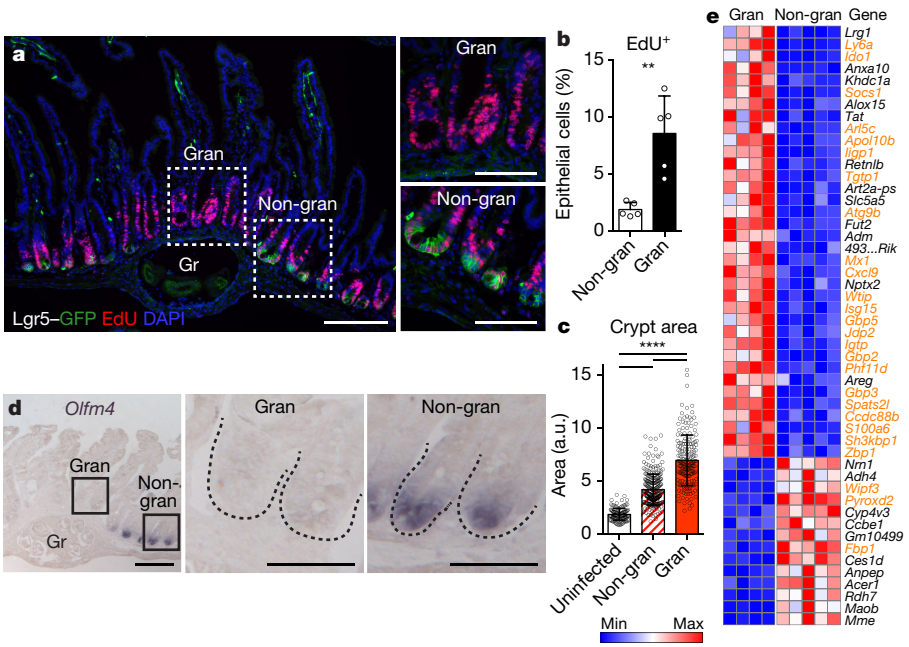


**Fig. 1 | Helminth infection induces an Lgr5$^-$ program in affected crypt epithelium.** Analysis of crypts overlying (gran) or adjacent to (non-gran) *H. polygyrus* granulomas (Gr) from day 6 of infection. **a**, Representative image of Lgr5–GFP and EdU staining in thin sections. **b**, Flow cytometry of EdU in biopsies of total epithelium. **c**, Crypt area from uninfected or infected (gran or non-gran) mice; a.u., arbitrary units. **d**, Representative image of in situ hybridization for *Olfm4* in thin sections. **e**, RNA-seq of sorted crypt epithelium from non-granuloma or granuloma biopsies. Data were filtered for ≥100 reads average in either group, FDR ≤ $10^{-4}$, and the 50 genes with the greatest fold-change are presented; high (red) and low (blue) relative expression. Gene names in orange are predicted IFN targets. *493…Rik*, RIKEN cDNA 4930461G14 gene (*4930461G14Rik*). $n = 5$ mice (**a**, **b**, **d**); 6 mice (**c**, uninfected); 15 mice (**c**, infected); 4 independently sorted samples (**e**, granuloma, 20 mice total), or 5 independently sorted samples (**e**, non-granuloma, 25 mice total). Statistics represent all biological replicates, and all experiments were replicated at least twice. Graphs show mean ± s.d. (**b**, **c**). $^{**}P < 0.01$, $^{****}P < 0.0001$ by unpaired, two-tailed Mann–Whitney test. Scale bars: main, 200 μm (**a** left, **d** left), 100 μm (magnified insets in **a**), 50 μm (insets in **d**).

[1]Biomedical Sciences Graduate Program, University of California, San Francisco, CA, USA. [2]Program in Craniofacial Biology and Department of Orofacial Sciences, University of California, San Francisco, CA, USA. [3]Howard Hughes Medical Institute and Departments of Medicine and Microbiology & Immunology, University of California, San Francisco, CA, USA. [4]Department of Molecular Oncology, Genentech Inc., South San Francisco, CA, USA. [5]Department of Pediatrics and Institute for Human Genetics, University of California, San Francisco, CA, USA. [6]These authors contributed equally: Ysbrand M. Nusse, Adam K. Savage. *e-mail: richard.locksley@ucsf.edu; ophir.klein@ucsf.edu

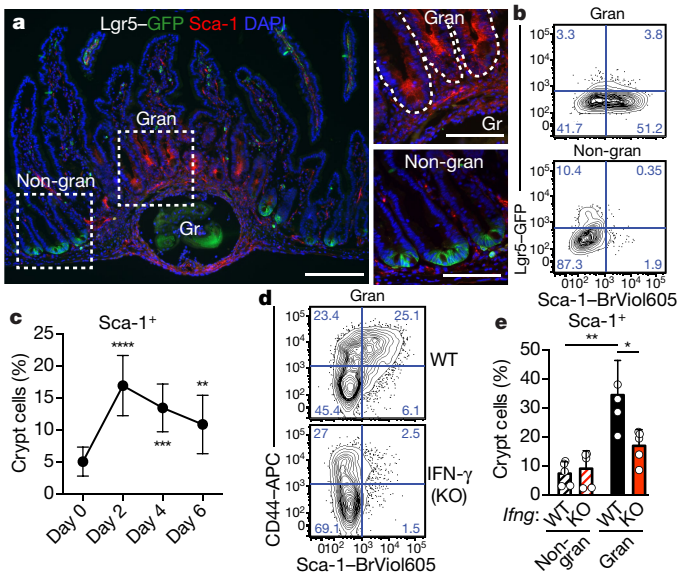


**Fig. 2 | IFN-γ mediates the helminth-induced crypt phenotype.** Day 6 of *H. polygyrus* infection, except as noted. **a**, Representative image of Lgr5–GFP and Sca-1 staining in crypts overlying (gran) or adjacent to (non-gran) granulomas (Gr). **b**, Representative flow cytometry of Lgr5–GFP and Sca-1 in crypt biopsies. **c**, Flow cytometry of Sca-1 in crypts from unfractionated epithelium following infection. **d**, Representative flow cytometry of CD44 and Sca-1 in epithelia from biopsies of IFN-γ-knockout (KO) mice. APC, allophycocyanin. **e**, Cells analysed as in (**d**). $n = 4$ (**b**), 5 (**a**, **d**, **e**), 8 (**c**, day 2, 4, 6), or 9 mice (**c**, day 0). Statistics represent all biological replicates, and all experiments were replicated at least twice. Graphs show mean ± s.d. (**c**, **e**). $^*P < 0.05$, $^{**}P < 0.01$, $^{***}P < 0.001$, $^{****}P < 0.0001$ by unpaired, two-tailed Mann–Whitney test. Scale bars: 200 μm (**a**, left), 100 μm (**a**, magnified insets).

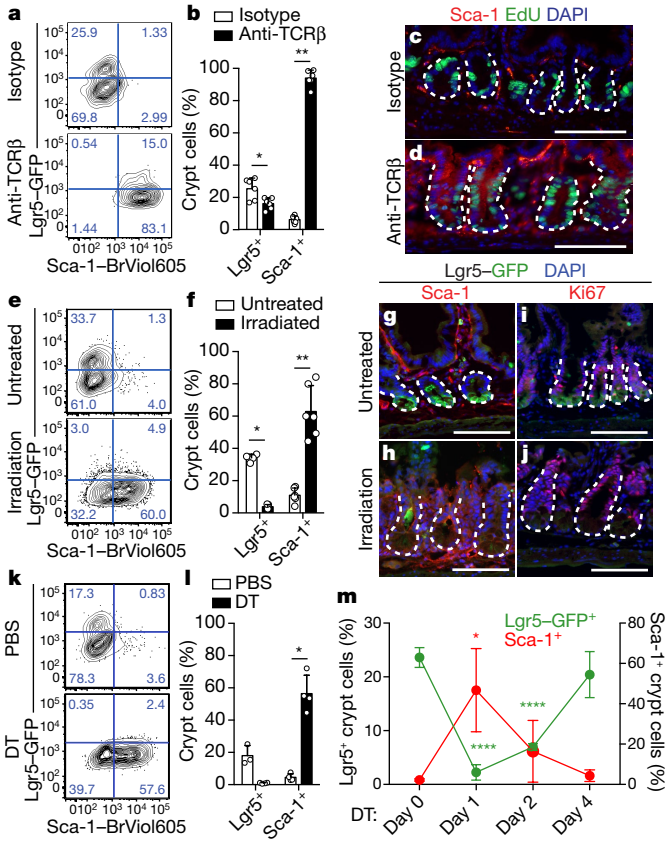


**Fig. 3 | The crypt response to *H. polygyrus* is a generalized response to tissue injury. a–d**, Mice were treated with 20 μg anti-TCRβ and analysed 24 h later by flow cytometry for Lgr5–GFP and Sca-1 in crypt cells (**a**, **b**) or for Sca-1 and EdU in thin sections (**c**, **d**). **e–j**, Mice were treated with 10 Gy irradiation and analysed at three days by flow cytometry and in thin sections for Lgr5–GFP and Sca-1 in crypt cells (**e–h**) or in thin sections for Lgr5–GFP and Ki67 (**i**, **j**). **k–m**, *Lgr5*$^{DTRGFP/+}$ mice were treated with diphtheria toxin (DT) and analysed by flow cytometry for Lgr5–GFP and Sca-1 in crypt cells at 24 h (**k**, **l**) or indicated time points (**m**). $n = 3$ (**g–l**, Lgr5, untreated; **m**, day 0), 4 (**c–f**, Lgr5, untreated; **k**, **l**, all others; **m**, day 1, 2, 4), 5 (**e**, **f**, Lgr5, irradiated), or 6 mice (**a**, **b**, **f**, Sca-1, irradiated). Statistics represent all biological replicates, and all experiments were replicated at least twice. Graphs show mean ± s.d. (**b**, **f**, **l**, **m**). $^*P < 0.05$, $^{**}P < 0.01$, $^{****}P < 0.0001$ by unpaired, two-tailed Mann–Whitney test (**b**, **f**, **l**) or unpaired, two-tailed *t*-tests (**m**). Scale bars: 100 μm (**c**, **d**, **g–j**).

(granuloma-associated crypts or GACs) were hyper-proliferative and enlarged (Fig. 1a–c, Extended Data Fig. 1a), as previously reported[5]. Notably, GACs did not express the Lgr5–GFP reporter (Fig. 1a, Extended Data Fig. 1b), whereas crypts not associated with granulomas still expressed Lgr5–GFP (Fig. 1a). *Olfm4*, another marker of intestinal stem cells (ISCs), was similarly repressed (Fig. 1d). In addition to loss of *Lgr5* and *Olfm4* expression, the Paneth cell marker MMP7 frequently co-stained with the goblet cell marker MUC2 (Extended Data Fig. 1c, d), as previously observed in helminth infections[6] and other perturbations of epithelial lineage commitment[7]. Thus, the epithelium overlying granulomas exhibits loss of ISC markers and disruption of the ISC niche[8].

To identify pathways in GACs that respond to *H. polygyrus* infection, we performed RNA sequencing analysis (RNA-seq) on purified crypt epithelium from punch biopsies of granulomas (Extended Data Fig. 2a). We identified 277 genes that were differentially expressed between biopsies of granuloma and non-granuloma crypts (Fig. 1e, Extended Data Fig. 2b, Supplementary Table 1). In addition to *Lgr5* and *Olfm4*, a suite of ISC signature genes[9] was downregulated in GACs (Extended Data Fig. 2c, d, Supplementary Table 2), confirming that *H. polygyrus* infection represses ISCs. Among the genes that were upregulated in GACs were an abundance of targets of interferon (IFN) signalling (Fig. 1e), and pathway analysis revealed an IFN response (Extended Data Fig. 2e, Supplementary Table 2).

One of the most highly upregulated genes was *Ly6a*, which encodes Sca-1, a surface protein that is associated with proliferative cells but is not present in humans. Sca-1 is a target of IFN signalling, and is induced in epithelia during colitis[10]. Immunofluorescence analysis showed that Sca-1 specifically marked Lgr5–GFP$^-$ GACs (Fig. 2a). Flow cytometry analysis confirmed that Sca-1 was enriched in GAC biopsies (Fig. 2b) and revealed that Sca-1 upregulation occurred as early as two days after infection (Fig. 2c, Extended Data Fig. 3a). Furthermore, Sca-1 expression was inversely correlated with that of Lgr5–GFP at all time points. Therefore, Sca-1 was a useful marker of crypt cells responding to *H. polygyrus*-driven epithelial disruption. By day 10 post-infection, diminished Sca-1 expression at granuloma remnants (Extended Data Fig. 3b) indicated that resolution had commenced. Another intestinal helminth, *Nippostrongylus brasiliensis*, which does not invade intestinal tissue, did not induce Sca-1 expression (Extended Data Fig. 3c), suggesting that Sca-1 expression is a specific response to crypt disruption.

Although helminths are typically associated with allergic immunity[11], our data pointed towards a role for IFN. We focused on IFN-γ, because elevated expression of this gene was found in granulomas of infected mice (Extended Data Fig. 3d), whereas type I and type III IFN transcripts were not induced in GACs (Extended Data Fig. 3e). We also found large numbers of neutrophils, which are known targets of IFN-γ[12], and an accumulation of IFN-γ$^+$ lymphocytes in granulomas (Extended Data Fig. 4a–d). Infection of IFN-γ-null mice with *H. polygyrus* showed that induction of Sca-1 (Fig. 2d, e) and IFN-target genes (Extended Data Fig. 4e) was dependent on IFN-γ; however, the Lgr5–GFP reporter remained downregulated in GACs of IFN-γ-null mice (Extended Data Fig. 4f). To assess the cell-autonomous effects of IFN-γ on intestinal epithelia, we deleted the IFN-γ receptor in intestinal epithelium and found a similar effect as with germline deletion of IFN-γ (Extended Data

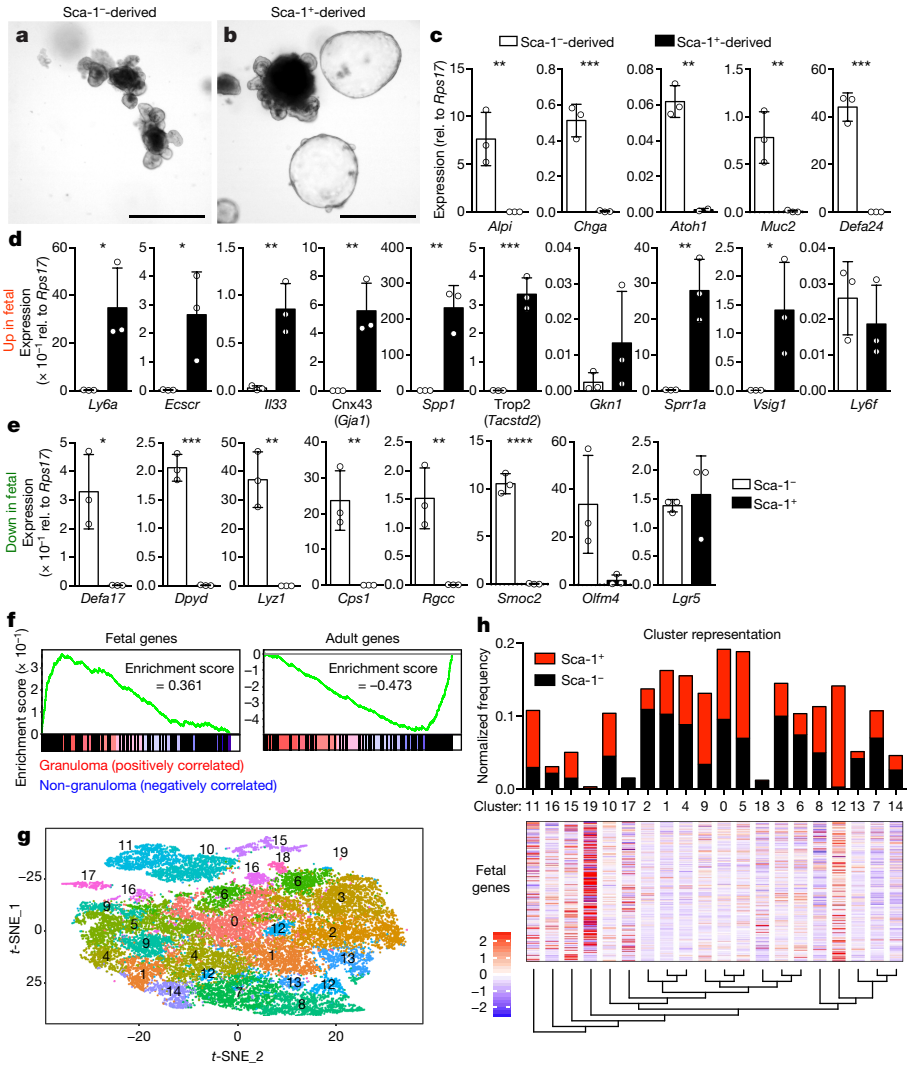


**Fig. 4 | Helminth-associated crypts acquire a fetal-like program.** **a**–**e**, Sorted Sca-1$^-$ (**a**) or Sca-1$^+$ (**b**) crypt cells from *H. polygyrus*-infected mice were cultured in organoid conditions, imaged after one passage (**a**, **b**), and analysed by quantitative PCR (qPCR) for markers of differentiated cells (**c**) or fetal-derived cultures[19] (**d**, **e**). **f**, Bulk RNA-seq data (as in Fig. 1e) were analysed by gene set enrichment analysis (GSEA) for cell signature genes[19]. All analyses have false discovery rate (FDR) $<10^{-3}$. **g**, **h**, Single-cell RNA-seq from $n = 19{,}754$ Sca-1$^-$ and $n = 6{,}669$ Sca-1$^+$ individually sorted crypt cells from one *H. polygyrus*-infected mouse. **g**, *t*-distributed stochastic neighbour embedding (*t*-SNE) distribution, colour coded to represent clusters identified independently by unsupervised hierarchical clustering. The relation of cluster identity to transcriptional signatures of mature lineages is shown in Extended Data Fig. 9. **h**, Sca-1$^-$ and Sca-1$^+$ cell frequency within each cluster, normalized to the total number of cells sequenced from each population (top). Normalized expression values for the fetal gene signature[19] were mapped to the clusters (middle) and arranged per the unsupervised dendrogram of cluster relatedness (bottom). $n = 3$ cultures from 3 mice (**c**–**e**), 4 independently sorted samples (**f**, granuloma, 20 mice total), 5 independently sorted samples (**f**, non-granuloma, 25 mice total), or 15 cultures from 15 mice (**a**, **b**). Statistics represent all biological replicates, and all experiments were replicated at least twice, except the single cell experiment, which was performed once. Graphs show mean ± s.d. (**c**–**e**). $^*P < 0.05$, $^{**}P < 0.01$, $^{***}P < 0.001$, $^{****}P < 0.0001$ by unpaired two-tailed *t*-tests. Scale bars: 500 μm (**a**, **b**).

Fig. 4g). Treating intestinal organoids with IFN-γ led to transcriptional changes corresponding to those found in GACs (Extended Data Fig. 4h). Together, these data demonstrate that immune cell-derived IFN-γ is a critical component of the GAC response.

Lymphocyte activation and IFN-γ production are elicited in other contexts of epithelial injury[13–15]. Therefore, we challenged uninfected mice with a monoclonal antibody (anti-TCRβ) that cross-links and activates the T cell receptor to assess the host response to immune cell activation. After 24 h, the level of *Ifng* transcript was increased (Extended Data Fig. 5a), and the intestinal epithelium broadly resembled the *H. polygyrus* GAC response, as indicated by reduction of Lgr5–GFP expression, induction of Sca-1, increased proliferation, increased crypt size (Fig. 3a–d, Extended Data Fig. 5b, c), and expression of a subset of *H. polygyrus*-activated transcriptional targets (Extended Data Fig. 5d).

The convergence of epithelial responses to immune cell activation following *H. polygyrus* infection and anti-TCRβ challenge might reflect a generalized reaction to tissue perturbation. To test this, we examined other tissue injury models. First, we lethally irradiated mice and analysed them after three days, at which time *Lgr5* expression is lost during regeneration[16,17]. We observed Sca-1 induction and an IFN response in crypt cells (Fig. 3e–h, Extended Data Fig. 5e, f), as well as continued proliferation (Fig. 3i, j) and increased crypt depth (Extended Data Fig. 5g), as previously reported[16].

Because irradiation is relatively non-specific, we sought to restrict cell death to the stem cell compartment by specifically ablating *Lgr5*-expressing cells[4]. Twenty-four hours after treatment of *Lgr5*$^{DTRGFP/+}$ mice with diphtheria toxin, Lgr5–GFP$^+$ cells were absent and Sca-1 was highly induced (Fig. 3k, l, Extended Data Fig. 6a, b). During recovery, Lgr5–GFP$^+$ ISCs re-emerged and Sca-1 expression decreased to

baseline levels (Fig. 3m). Notably, ablation of Lgr5$^+$ cells did not induce crypt hyperplasia (Extended Data Fig. 6c) or GAC-like expression of some IFN targets (data not shown), showing that there is a distinction between the Sca-1 response following *Lgr5* ablation and the response to other types of epithelial disruption. However, IFN activation has been observed after ablation of Lgr5$^+$ cells in tumours[18]. Therefore, diverse insults that disrupt Lgr5$^+$ cells induce GAC-like responses during regeneration.

Lgr5$^+$ cells are required for regeneration after irradiation-induced injury[17]. To test whether they are also required for the *H. polygyrus*-induced GAC phenotype, we ablated Lgr5$^+$ cells immediately before infection. In this setting, although we confirmed that GAC cells were part of the Lgr5$^+$ ISC lineage hierarchy (Extended Data Fig. 6d, e), crypt cell frequency, Sca-1 induction, and 5-ethynyl-2′-deoxyuridine (EdU) incorporation were unaffected (Extended Data Fig. 6f–k). These data indicate that whereas the *H. polygyrus*-induced GAC phenotype is mediated by progeny of ISCs, it can occur independently of Lgr5$^+$ ISCs.

Sca-1$^+$ GAC cells were hyper-proliferative and gave rise to granuloma-associated villus epithelium (Extended Data Fig. 7a, b). To assess the regenerative capacity of GACs, we sorted Sca-1$^+$ and Sca-1$^-$ crypt cells from *H. polygyrus*-infected mice and cultured them under standard organoid conditions. Whereas Sca-1$^-$ cells formed typical organoids (Fig. 4a), Sca-1$^+$ cells formed large, smooth spheroids that were devoid of crypt budding (Fig. 4b) and could be stably passaged for more than six months (data not shown). Sca-1$^+$ spheroids lost expression of markers of differentiated epithelium (Fig. 4c), suggesting that they reflected growth of an undifferentiated cell type. Spheroids have been observed in high-Wnt conditions[8]; however, in our studies, we did not add exogenous Wnt, and we found no difference in *Axin2* expression between Sca-1$^+$ and Sca-1$^-$ cultures (Extended Data Fig. 8a), suggesting that Wnt signalling is not hyperactive in Sca-1$^+$ spheroids. Recent work[19,20] has demonstrated that cultured fetal epithelium also forms spheroids. We therefore tested expression of fetal epithelial markers and found that nearly all fetal genes assayed were highly expressed in Sca-1$^+$ cultures (Fig. 4d, e). Like fetal cultures[20], Sca-1$^+$ spheroids were not sensitive to R-Spondin1 withdrawal (data not shown). Therefore, Sca-1$^+$ cells adopted a state in vitro that was distinct from Sca-1$^-$ cells and exhibited characteristics of fetal intestinal epithelium.

We sought to determine whether the fetal program was activated in vivo and found that the fetal markers *Gja1* and *Spp1* were upregulated in GACs during *H. polygyrus* infection (Extended Data Fig. 8b). Furthermore, Sca-1 was expressed in mouse fetal intestinal epithelium at embryonic day 15.5 (Extended Data Fig. 8c). This remarkable similarity led us to re-analyse the results of our RNA-seq of GAC epithelium. We found strong enrichment of the fetal signature in GAC epithelium, whereas the adult signature was enriched in non-GACs (Fig. 4f, Supplementary Table 2). Furthermore, the signatures[21] of stem cells, enterocytes and Paneth cells, but not goblet cells, were lost in GACs (Extended Data Fig. 8d, Supplementary Table 2). Taken together, these data indicate that, during infection, GACs adopt an undifferentiated state resembling the fetal epithelium.

Enrichment of the goblet cell signature in GAC epithelium suggests that there is heterogeneity within the pool of Sca-1$^+$ cells. To investigate whether a subgroup of cells underpin the fetal signature, we performed single-cell RNA-seq of Sca-1$^+$ and Sca-1$^-$ crypt cells. Unsupervised clustering of the merged datasets revealed that most cell clusters were composed of both Sca-1$^+$ and Sca-1$^-$ cells (Fig. 4g, h) and, although we excluded mature epithelium, the transcriptional signature of specific lineages could be recognized in some clusters (Extended Data Fig. 9, Supplementary Table 4). We focused on cluster 12, which consisted almost entirely of Sca-1$^+$ cells (98.2%). By overlaying known intestinal cell type signatures[19,21], we found that cluster 12 was depleted of mature cell markers (Extended Data Fig. 9), and was strongly enriched for the fetal program (Fig. 4h, Supplementary Table 5), suggesting that this cluster represents a unique cell identity within the larger Sca-1$^+$ pool that is elicited by *H. polygyrus* infection.

Intestinal crypts have been postulated to respond to damage by activation of reserve stem cells[16,22] or reacquisition of stemness by differentiated progenitors[23–25]. Here, our use of an evolutionarily adapted parasite led to identification of a novel infection-mediated alteration of the crypt in response to injury. By monitoring the markers Lgr5–GFP and Sca-1, we found that an overlapping injury-response program was induced by other tissue-damaging agents, indicating a generalized strategy by which the intestine responds to stress. Our data identify a novel cell type that arises in the damaged crypts and suggest that crypt repair repurposes aspects of fetal development in order to restore integrity of the intestinal barrier. Indeed, a re-activation of fetal markers has been observed in models of injury in other tissues[26–28]. Furthermore, a recent report examining a chemical colitis model also uncovered induction of Sca-1 and a fetal signature in regenerative colonic crypts[29]. This work showed that extracellular matrix-driven activation of Yap–Taz signalling was linked to regeneration, whereas we found a discrete subset of Sca-1$^+$ crypt cells associated with a fetal gene signature. These complementary studies suggest that induction of the fetal program may be a core response to injury in the crypt. Taken together, the helminth-induced changes in crypt epithelia that we discovered point to a repurposing of some of the functional capabilities of the developing fetal gut and highlight a novel mechanism of repair in the intestinal crypt that involves infection-induced developmental plasticity.

## Online content

Any Methods, including any statements of data availability and Nature Research reporting summaries, along with any additional references and Source Data files, are available in the online version of the paper at https://doi.org/10.1038/s41586-018-0257-1.

Received: 23 March 2017; Accepted: 9 May 2018;
Published online 27 June 2018.

1. Karin, M. & Clevers, H. Reparative inflammation takes charge of tissue regeneration. *Nature* **529**, 307–315 (2016).
2. Maizels, R. M. et al. Immune modulation and modulators in *Heligmosomoides polygyrus* infection. *Exp. Parasitol.* **132**, 76–89 (2012).
3. Barker, N. et al. Identification of stem cells in small intestine and colon by marker gene *Lgr5*. *Nature* **449**, 1003–1007 (2007).
4. Tian, H. et al. A reserve stem cell population in small intestine renders Lgr5-positive cells dispensable. *Nature* **478**, 255–259 (2011).
5. Ferguson, A. & Jarrett, E. E. Hypersensitivity reactions in small intestine. I Thymus dependence of experimental 'partial villous atrophy'. *Gut* **16**, 114–117 (1975).
6. Kamal, M. et al. Paneth and intermediate cell hyperplasia induced in mice by helminth infections. *Parasitology* **125**, 275–281 (2002).
7. VanDussen, K. L. et al. Notch signaling modulates proliferation and differentiation of intestinal crypt base columnar stem cells. *Development* **139**, 488–497 (2012).
8. Sato, T. et al. Paneth cells constitute the niche for Lgr5 stem cells in intestinal crypts. *Nature* **469**, 415–418 (2011).
9. Muñoz, J. et al. The Lgr5 intestinal stem cell signature: robust expression of proposed quiescent '+4' cell markers. *EMBO J.* **31**, 3079–3091 (2012).
10. Flanagan, K. et al. Intestinal epithelial cell up-regulation of LY6 molecules during colitis results in enhanced chemokine secretion. *J. Immunol.* **180**, 3874–3881 (2008).
11. Grencis, R. K. Immunity to helminths: Resistance, regulation, and susceptibility to gastrointestinal nematodes. *Annu. Rev. Immunol.* **33**, 201–225 (2015).
12. Amulic, B., Cazalet, C., Hayes, G. L., Metzler, K. D. & Zychlinsky, A. Neutrophil function: From mechanisms to disease. *Annu. Rev. Immunol.* **30**, 459–489 (2012).
13. Miura, N. et al. Anti-CD3 induces bi-phasic apoptosis in murine intestinal epithelial cells: possible involvement of the Fas/Fas ligand system in different T cell compartments. *Int. Immunol.* **17**, 513–522 (2005).
14. Sollid, L. M. & Jabri, B. Triggers and drivers of autoimmunity: lessons from coeliac disease. *Nat. Rev. Immunol.* **13**, 294–302 (2013).
15. Zhou, P., Streutker, C., Borojevic, R., Wang, Y. & Croitoru, K. IL-10 modulates intestinal damage and epithelial cell apoptosis in T cell-mediated enteropathy. *Am. J. Physiol. Gastrointest. Liver Physiol.* **287**, G599–G604 (2004).
16. Yan, K. S. et al. The intestinal stem cell markers Bmi1 and Lgr5 identify two functionally distinct populations. *Proc. Natl Acad. Sci. USA* **109**, 466–471 (2011).
17. Metcalfe, C., Kljavin, N. M., Ybarra, R. & de Sauvage, F. J. Lgr5$^+$ stem cells are indispensable for radiation-induced intestinal regeneration. *Cell Stem Cell* **14**, 149–159 (2014).
18. Melo, F. de S. E. et al. A distinct role for Lgr5$^+$stem cells in primary and metastatic colon cancer. *Nature* **543**, 676–680 (2017).
19. Mustata, R. C. et al. Identification of Lgr5-independent spheroid-generating progenitors of the mouse fetal intestinal epithelium. *Cell Reports* **5**, 421–432 (2013).

20. Fordham, R. P. et al. Transplantation of expanded fetal intestinal progenitors contributes to colon regeneration after injury. *Cell Stem Cell* **13**, 734–744 (2013).
21. Haber, A. L. et al. A single-cell survey of the small intestinal epithelium. *Nature* **551**, 333–339 (2017).
22. Asfaha, S. et al. Krt19$^{+}$/Lgr5$^{-}$ cells are radioresistant cancer-initiating stem cells in the colon and intestine. *Cell Stem Cell* **16**, 627–638 (2015).
23. van Es, J. H. et al. Dll1$^{+}$ secretory progenitor cells revert to stem cells upon crypt damage. *Nat. Cell Biol.* **14**, 1099–1104 (2012).
24. Tetteh, P. W. et al. Replacement of lost Lgr5-positive stem cells through plasticity of their enterocyte-lineage daughters. *Cell Stem Cell* **18**, 203–213 (2016).
25. Buczacki, S. J. A. et al. Intestinal label-retaining cells are secretory precursors expressing Lgr5. *Nature* **495**, 65–69 (2013).
26. Fernandez Vallone, V. et al. Trop2 marks transient gastric fetal epithelium and adult regenerating cells after epithelial damage. *Development* **143**, 1452–1463 (2016).
27. Gadye, L. et al. Injury activates transient olfactory stem cell states with diverse lineage capacities. *Cell Stem Cell* **21**, 775–790 (2017).
28. Lin, B. et al. Injury induces endogenous reprogramming and dedifferentiation of neuronal progenitors to multipotency. *Cell Stem Cell* **21**, 761–774 (2017).
29. Yui, S. et al. Yap/Taz-dependent reprogramming of colonic epithelium links ECM remodeling to tissue regeneration. *Cell Stem Cell* **22**, 35–49 (2018).

**Acknowledgements** We thank M. Consengco, R. D'Urso, J. Ming, A. Rathnayake, N. Wang and Z. Wang for technical expertise, the UCSF Institute of Human Genetics Core and Functional Genomics Core for performing the RNA-seq experiments, members of the Klein and Locksley labs for discussions, and K. Lindquist for advice on GSEA analysis. This work was supported by the National Institutes of Health (AI026918, AI030663 and U01DK103147 from the Intestinal Stem Cell Consortium—a collaborative research project funded by the National Institute of Diabetes and Digestive and Kidney Diseases and the National Institute of Allergy and Infectious Diseases), the Howard Hughes Medical Institute (HHMI), the California Institute for Regenerative Medicine (RN3-06525) and the Sandler Asthma Basic Research Center at the University of California, San Francisco. A.K.S. is an HHMI Fellow. Y.M.N. was awarded a Genentech Graduate Fellowship in 2014.

**Reviewer information** *Nature* thanks A. Hanash, T. Sato, S. Takashima and the other anonymous reviewer(s) for their contribution to the peer review of this work.

**Author contributions** Y.M.N. and A.K.S. jointly conceived the study and designed, performed and interpreted histology, cytometry, transcriptomic and culture experiments. P.M. performed computational analysis of the single-cell transcriptomic experiment. A.K.M.R.-H. and T.A.L. performed and interpreted histology experiments. F.J.d.S. contributed essential reagents. O.D.K. and R.M.L. directed the study and wrote the manuscript with Y.M.N. and A.K.S.

**Competing interests** F.J.d.S. is an employee of Genentech and owns shares in Roche.

**Additional information**
**Extended data** is available for this paper at https://doi.org/10.1038/s41586-018-0257-1.
**Supplementary information** is available for this paper at https://doi.org/10.1038/s41586-018-0257-1.
**Reprints and permissions information** is available at http://www.nature.com/reprints.
**Correspondence and requests for materials** should be addressed to R.M.L. and O.D.K.

## METHODS

**Mice.** Mice were maintained in the University of California San Francisco (UCSF) specific pathogen-free animal facility in compliance with all ethical guidelines established by the Institutional Animal Care and Use Committee and Laboratory Animal Resource Center. All experimental procedures were approved by the Laboratory Animal Resource Center at UCSF. Both male and female mice aged 6–14 weeks were used for all experiments, except those analysing fetal tissue. Mice were chosen for experimental conditions randomly but without formal randomization. Investigators were blinded where possible, but this was frequently precluded owing to inherent facets of infection experiments. *Lgr5*$^{DTRGFP}$ mice were previously described[4]. Wild-type (C57BL/6J), *Lgr5*$^{GFP\text{-}creERT2/+}$ (B6.129P2-*Lgr5*$^{tm1(cre/ERT2)Cle}$/J), *Rosa26*$^{RFP/+}$ (B6;129S6-*Gt(ROSA)26Sor*$^{tm14(CAG\text{-}tdTomato)Hze}$/J), IFN-γ reporter (B6.129S4-*Ifng*$^{tm3.1Lky}$/J), IFN-γ-null (B6.129S7-*Ifng*$^{tm1Ts}$/J), IFN-γ receptor-flox (*Ifngr1*$^{loxP/loxP}$; C57BL/6N-*Ifngr1*$^{tm1.1Rds}$/J), and Vil1-cre (B6.Cg-Tg(Vil1-cre)997Gum/J) mice were from The Jackson Laboratory and were maintained on a C57BL/6 background. For analysis of embryonic tissue, timed matings were established, and the morning after plugs were recognized was considered embryonic stage (e) 0.5. Fetal intestine was dissected at the time points indicated.

**Helminth infection and treatments.** Mice were infected by oral gavage with 200 *H. polygyrus* L3 larvae and were killed at the indicated time points. For anti-TCRβ treatment, mice were administered with 20 μg per mouse of clone H57 TCRβ monoclonal antibody and analysed 24 h later. For irradiation, mice were exposed to 10 Gy and analysed approximately 72 h later. For ablation of Lgr5$^{+}$ cells, *Lgr5*$^{DTRGFP/+}$ mice were administered 50 μg/kg diphtheria toxin intraperitoneally and analysed at the indicated time points. For determination of cell proliferation, 500 μg EdU was administered intraperitoneally 1 h before mice were killed, except for Extended Data Fig. 7b, where EdU was administered 24 h before mice were killed. For lineage tracing experiments, *Lgr5*$^{GFP\text{-}creERT2/+}$ *Rosa26*$^{RFP/+}$ mice were infected with *H. polygyrus* and injected with 2.5 mg tamoxifen in corn oil intraperitoneally at the indicated time points and analysed at day 6.

**Tissue preparation and flow cytometry.** Preparation of intestinal tissue for flow cytometry was modified from previous work[30]. The duodenum was dissected, flushed extensively with cold PBS, and the mesenteric tissue was removed. For whole tissue preps, Peyer's patches were removed and tissue was turned inside out. For recovery of punch biopsies, tissue was filleted open longitudinally. In both cases, tissue was shaken in three changes of 20 ml cold PBS and washed for 20 min at 37 °C in two changes of 20 ml $Ca^{2+}$/$Mg^{2+}$-free HBSS containing 5 mM DTT, 10 mM HEPES and 2% FCS, followed by 20 ml of $Ca^{2+}$/$Mg^{2+}$-replete HBSS containing 10 mM HEPES and 2% FCS. For punch biopsies, granuloma and non-granuloma tissues were dissected with a 1-mm punch tool under low-power magnification. Tissues were digested for 30 min at 37 °C in 5 ml (whole tissue) or 2 ml (punch biopsies) $Ca^{2+}$/$Mg^{2+}$-replete HBSS containing 10 mM HEPES, 2% FCS, 30 μg/ml DNaseI (Roche) and 0.1 Wünsch units/ml Liberase TM (Roche), and whole tissue was homogenized in C tubes using a gentleMACS tissue dissociator (Miltenyi). Homogenate or punch biopsies were passed through a 100-μm filter with assistance of a 3-ml syringe plunger, and enumerated for staining equivalent numbers for flow cytometry or sorting. Fc Block (anti-CD16/32), doublet exclusion, and DAPI exclusion were used in all cases. Data were acquired with a Becton Dickinson Fortessa and analysed using FlowJo (Tree Star). Cell sorting was performed with a Beckman Coulter MoFlo XDP.

**Immunofluorescence and in situ hybridization.** For tissue staining in section, mice were perfused with cold 4% PFA in PBS. The proximal 10 cm of duodenum was cleaned, flushed with cold 4% PFA, and fixed in 4% PFA for 4 h at 4 °C. The tissue was cryo-protected in 30% sucrose overnight at 4 °C. Samples were embedded in OCT and 8-μm sections were prepared for immunofluorescence staining. For immunohistochemistry and in situ hybridization, the samples were fixed overnight in 4% PFA, paraffin embedded, and sectioned at 5 μm for immunohistochemistry or 10 μm for in situ hybridization. For crypt area quantification, crypts clearly above distended granuloma tissue containing visible larval worms were called as 'granuloma' and others were called 'non-granuloma'. Crypt area was quantified in ImageJ. For fetal whole mount imaging, fetal intestines were fixed in 4% PFA in PBS for 3 h, permeabilized, and blocked for 4 h at room temperature. Primary and secondary antibodies were incubated at 4 °C overnight. Images were acquired and processed with a Leica DM5000 B or a Zeiss Axio Imager 2 and Adobe Photoshop.

**In situ hybridization.** An *Olfm4* probe was designed by PCR amplifying an 898-bp sequence from total intestinal cDNA using the primers 5′-AACCTG ACGGTCCGAGTAGA-3′ (forward) and 5′-TGCTGGCCTCAGTTGCATAA-3′ (reverse). *Olfm4* cDNA was cloned into a pGEM-T Easy vector (Promega). *Olfm4* antisense probes were prepared and in situ hybridization was performed as described[31].

**Bulk RNA sequencing.** Five wild-type mice were infected with *H. polygyrus* and six days later 1-mm punch biopsies from granuloma and non-granuloma tissue were taken, pooled by tissue, digested, and sorted for DAPI$^{lo}$ CD45$^{-}$ EpCAM$^{+}$ CD44$^{+}$ crypt epithelium. RNA from six granuloma (30 mice total) and five non-granuloma (25 mice total) sorts was submitted for RNA sequencing. Two granuloma datasets were excluded owing to low unique mapping rates and failure to group by tissue in principle components analysis and hierarchical clustering. The remaining data were filtered for a combination of minimum read count, false discovery rate, and fold-change comparison, as indicated in figure legends. Heat maps were generated using Morpheus (https://software.broadinstitute.org/morpheus/) and upstream regulators were determined using Ingenuity Pathways Analysis (Qiagen). Predicted mouse IFN targets were determined using Interferome (http://interferome.its.monash.edu.au/interferome) with default settings. GSEA analysis[32] was done with 1000 permutations by gene set. The expression dataset was generated by filtering out low abundance genes. Hallmark gene sets were obtained from the Broad MSigDB[33]. Additional gene sets were generated from published datasets[9,19,21]. The gene-filtered expression data are available in Supplementary Table 1 and the GSEA analysis results and input files are available in Supplementary Table 2.

**Single-cell RNA-seq.** Sca-1$^{+}$ or Sca-1$^{-}$ crypt cells were sorted from one mouse infected with *H. polygyrus* for six days. The two resulting cell suspensions (~70,000 cells each) were submitted as separate samples to be barcoded for single-cell RNA-seq using the Chromium Controller (10X Genomics) and the Single Cell 3′ Library Kit v2 (PN-120236/37/62). Resulting libraries were sequenced on a HiSeq 4000 (Illumina) using HiSeq 4000 PE Cluster Kit (PN PE-410-1001) with HiSeq 4000 SBS Kit (150 cycles, PN FC-410-1002), with one sample being loaded per sequencing lane. 19,834 Sca-1$^{-}$ cells (approximately 15,000 reads per cell) and 7,354 Sca1$^{+}$ cells (approximately 40,000 reads per cell) were successfully barcoded and their transcriptomes were sequenced. Raw sequencing data were processed for initial QC analysis and alignment by our sequencing core (Institute of Human Genetics, UCSF) using Cell Ranger software. Further analysis of differential gene expression and unsupervised hierarchical clustering were performed using the Seurat package (v2.0)[34,35]. Samples were merged after read depth correction and the combined dataset was filtered to exclude cells expressing less than 200 genes. Additionally, genes detected in fewer than 10 cells were removed from the analysis. Variable gene expression was assessed in the filtered data set after correction for mitochondrial gene expression. Linear reduction of the data was performed using principle components analysis, focusing on the first 15 principle components determined to be significant to explain variation in the data set via a large permutation test. Cells were clustered using the function FindClusters with a resolution parameter of 2.0. Graphical representation was achieved using the *t*-SNE algorithm, upon which the independently identified clusters were colour coded. Published lists[19,21] of markers for various intestinal crypt cell types were visualized on the clusters with the DoHeatmap function of the Seurat package. For analysis of cluster contribution by Sca-1$^{+}$ or Sca-1$^{-}$ crypt cells (Fig. 4h), cell numbers were first normalized to the total number sequenced for each population. We considered cluster 19 to be an aberrant cluster owing to low cell number (33 of 26,423 total), enrichment for multiple intestinal lineages, and isolation in *t*-SNE analysis. The mean normalized expression values by cluster are available in Supplementary Table 3 and mean normalized expression values presented in the heat maps are available in Supplementary Table 4. The hypergeometric test for enrichment of the fetal gene program signature within each cluster is available in Supplementary Table 5.

**Antibodies.** The following antibodies (BioLegend) were used for flow cytometry: CD45 (30-F11), CD326/EpCAM (G8.8), CD44 (IM7), Sca-1 (D7), TCRβ (H57), γδTCR (GL3), NK1.1 (PK136), CD90.2 (53-2.1), CD11b (M1/70) and Gr1 (RB6-8C5). For immunofluorescence staining of sections, the following antibodies were used: GFP (GFP-1020, Aves; ab13790, Abcam), Ki67 (Sp6, Thermo Fischer Scientific), E-cadherin (24E10, Cell Signaling Technology), Sca-1 (e13-161.7, Biolegend), Muc2 (SC-15334, Santa Cruz Biotechnology), Mmp7 (AF2967, R&D Systems). EdU was detected using Click-iT Plus EdU Assay Kit (ThermoFisher).

**Organoid culture.** Cultures from sorted single cells were established as described[36]. In brief, CD45$^{-}$ EpCAM$^{+}$ CD44$^{+}$ Sca-1$^{+}$ and Sca-1$^{-}$ cells were sorted into PBS containing 10% FCS. Cells were re-suspended in GFR, phenol-free Matrigel (Fisher) supplemented with 500 ng/ml EGF (Sigma-Aldrich), 1 μg/ml Noggin (R&D Sytems), 10 μM Jagged-1 peptide (Anaspec) and 10% R-Spondin1 Conditioned Medium (gift of N. Shroyer). Fifty microlitres of Matrigel containing cells was plated in a 24-well cell culture plate, and left to set at 37 °C for 15 min. Pre-warmed 37 °C ENR Medium (Advanced DMEM/F12, 10 mM HEPES, 1X GlutaMAX, 1% Pen/Strep, 1X N-2 Supplement, 1X B-27 Supplement, 1 mM N-Acetylcysteine, 100 ng/ml Noggin, 50 ng/ml EGF, 5% R-Spondin1 Conditioned Media) with 2.5 μM CHIR99021, 2.5 μM Thiazovinin, and 1 μM Jagged-1 peptide was overlaid. Cells were cultured at 37 °C. After three days, the medium was exchanged for ENR medium without CHIR99021, Thiazovinin, or Jagged-1 peptide. Cultures were passaged after eight days and then every 5–7 days thereafter with growth factor-free Matrigel. Cultures were typically analysed at the end of the first passage by imaging and qPCR. Some qPCR experiments were conducted on established cultures, such as in Fig. 4c–e. For in vitro IFN-γ treatment, wild-type organoid lines were prepared from whole crypts and treated three days after passage by exchanging the standard organoid medium with fresh organoid medium

containing 5 ng/ml IFN-γ (485-MI, R&D Systems). Twenty-four hours later, organoids were harvested by centrifugation, aspirating the media and Matrigel, and lysed using RLT buffer (Qiagen).

**Quantitative PCR.** RNA from 5-mm whole tissue (after QIAshredder), sorted cells, or organoids was extracted using RNeasy Mini or Micro Kits (Qiagen). cDNA was synthesized with High Capacity cDNA Reverse Transcription Kits (Applied Biosystems). qPCR reactions were performed using Power SYBR Green (Invitrogen) on an Applied Biosystems StepOnePlus for whole tissue, or iTaq Universal SYBR Green Supermix (Bio Rad) in 384-well plates on a QuantStudio 6 Flex Real-Time PCR System (Thermo Fisher Scientific) for sorted cells and organoids. Primers used for qPCR are listed in Supplementary Table 6.

**Statistics.** Except in Extended Data Fig. 4h, all data points are biological replicates, not formally randomly assigned. The investigators were not formally blinded to allocation during experiments and outcome assessment. All experiments were independently replicated with similar results at least twice, except in Extended Data Fig. 6a, b and the single-cell RNA-seq experiment, which were both performed once. No data were excluded, except in the bulk RNA-seq experiment, as noted in the Methods. No statistical methods were used to predetermine sample size and differences in intra-sample variances were present. Statistical significance was determined in Prism (GraphPad Software) using an unpaired, two-tailed Mann–Whitney test without multiple comparisons correction, except for the use of unpaired, two-tailed *t*-tests in Fig. 3m and Fig. 4c–e, as noted in the legend. Bar charts indicate the mean of samples and error bars represent ± s.d. of the mean. $*P<0.05$, $**P<0.01$, $***P<0.001$, $****P<0.0001$. Hypergeometric tests were performed using GeneProf[37].

**Reporting summary.** Further information on experimental design is available in the Nature Research Reporting Summary linked to this paper.

**Data availability.** The RNA-seq data reported in this study are available at the Gene Expression Omnibus under accession codes GSE97405 (bulk) and GSE108233 (single-cell). The source data for all charts are available in the online version of the paper.


30. Goodyear, A. W., Kumar, A., Dow, S. & Ryan, E. P. Optimization of murine small intestine leukocyte isolation for global immune phenotype analysis. *J. Immunol. Methods* **405**, 97–108 (2014).
31. Gregorieff, A. & Clevers, H. in *Current Protocols in Stem Cell Biology* (John Wiley & Sons, 2015).
32. Subramanian, A. et al. Gene set enrichment analysis: a knowledge-based approach for interpreting genome-wide expression profiles. *Proc. Natl Acad. Sci. USA* **102**, 15545–15550 (2005).
33. Liberzon, A. et al. The molecular signatures database (MSigDB) hallmark gene set collection. *Cell Syst.* **1**, 417–425 (2015).
34. Macosko, E. Z. et al. Highly parallel genome-wide expression profiling of individual cells using nanoliter droplets. *Cell* **161**, 1202–1214 (2015).
35. Satija, R., Farrell, J. A., Gennert, D., Schier, A. F. & Regev, A. Spatial reconstruction of single-cell gene expression data. *Nat. Biotechnol.* **33**, 495–502 (2015).
36. Mahe, M. M. et al. Establishment of gastrointestinal epithelial organoids. *Curr. Protoc. Mouse Biol.* **3**, 217–240 (2013).
37. Halbritter, F., Vaidya, H. J. & Tomlinson, S. R. GeneProf: analysis of high-throughput sequencing experiments. *Nat. Methods* **9**, 7–8 (2011).

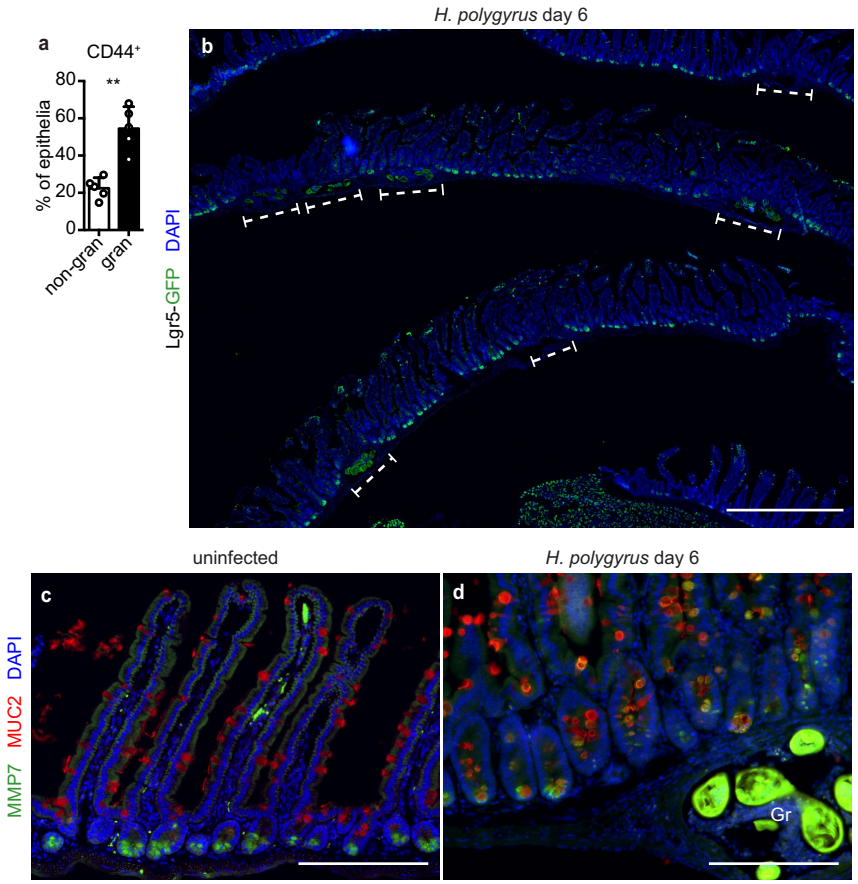


**Extended Data Fig. 1 | Helminth infection alters the crypt and intestinal stem cell niche.** Day 6 of *H. polygyrus* infection. **a**, Flow cytometry of $CD44^+$ epithelium from non-granuloma or granuloma biopsies. **b**, Representative image of Lgr5–GFP staining in the duodenum. Granulomas are indicated by the dashed brackets. In some granulomas, the helminth larva is recognizable by autofluorescence. The presence of rare Lgr5–GFP negative crypts is likely to be a sectioning artefact. **c**, **d**, MMP7 and MUC2 staining in normal duodenum or duodenum from mice infected with *H. polygyrus*. Gr, granuloma. $n = 3$ (**b**), or 5 mice (**a**, **c**, **d**). Statistics represent all biological replicates, and all experiments were replicated at least twice. Graphs show mean ± s.d. (**a**). $^{**}P < 0.01$ by unpaired, two-tailed Mann–Whitney test. Scale bars: 1 mm (**b**), 200 μm (**c**, **d**).

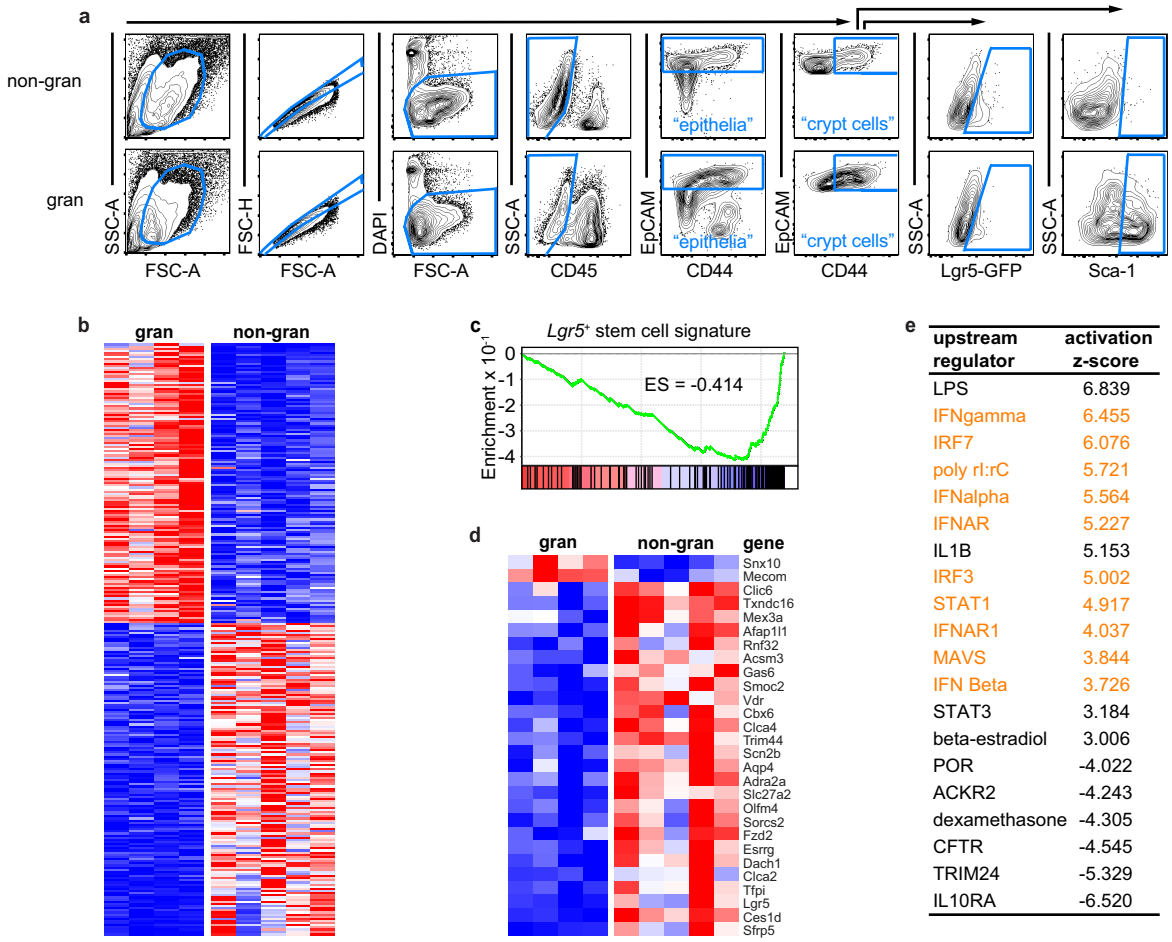


e

| upstream regulator | activation z-score |
|---|---|
| LPS | 6.839 |
| IFNgamma | 6.455 |
| IRF7 | 6.076 |
| poly rI:rC | 5.721 |
| IFNalpha | 5.564 |
| IFNAR | 5.227 |
| IL1B | 5.153 |
| IRF3 | 5.002 |
| STAT1 | 4.917 |
| IFNAR1 | 4.037 |
| MAVS | 3.844 |
| IFN Beta | 3.726 |
| STAT3 | 3.184 |
| beta-estradiol | 3.006 |
| POR | -4.022 |
| ACKR2 | -4.243 |
| dexamethasone | -4.305 |
| CFTR | -4.545 |
| TRIM24 | -5.329 |
| IL10RA | -6.520 |

**Extended Data Fig. 2 | RNA-seq analysis of granuloma-associated crypt epithelium. a**, Representative gating example of epithelia, crypt cells, Lgr5–GFP and Sca-1 in biopsied tissue six days after *H. polygyrus* infection. Unfractionated tissue preps (as in Extended Data Fig. 3a) were gated similarly. **b**–**e**, Crypt epithelium was sorted from granuloma and non-granuloma biopsies and subjected to RNA-seq analysis as indicated in the Methods. **b**, The data were filtered for $\geq$100 reads average in either group, FDR $\leq$ 0.05, and fold-change comparison of $\geq$ 2. The 277 genes that passed were compiled into a heat map demonstrating high (red) and low (blue) relative expression. **c**, GSEA for Lgr5$^+$ signature genes[9]. FDR <0.01. ES, enrichment score. **d**, Lgr5$^+$ intestinal stem cell signature genes[9] were cross-referenced to the RNA-seq dataset. Data were filtered as in (**b**) except no fold-change requirement was applied. *Clca4* is also known as *Clca3b* **e**, The unfiltered RNA-seq dataset was analysed for upstream regulators using Ingenuity Pathways Analysis. The activation *Z* score indicates the extent of enrichment of targets within the RNA-seq dataset downstream of the indicated regulator, with a positive score indicating enrichment. IFN-related pathways are highlighted in orange. $n = 4$ independently sorted samples (**b**–**e**, granuloma, 20 mice total), or 5 independently sorted samples (**b**–**e**, non-granuloma, 25 mice total).

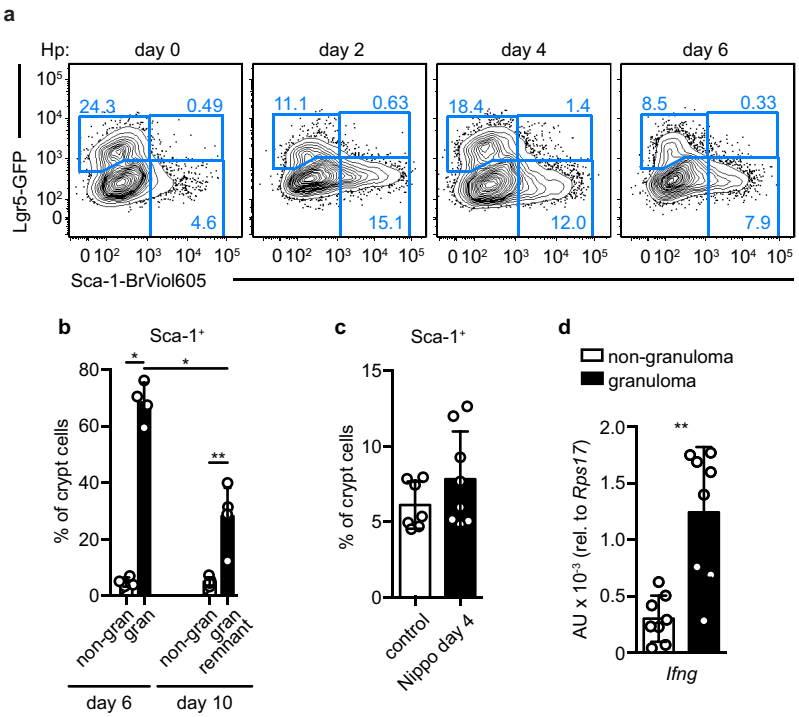


**e**

| gene | fold change (gran/non-gran) | mean granuloma read count | mean non-granuloma read count |
|---|---|---|---|
| Ifna-ps1 | NA | 0.00 | 0.00 |
| Ifna1 | NA | 0.00 | 0.00 |
| Ifna2 | NA | 0.00 | 0.00 |
| Ifna4 | NA | 0.00 | 0.00 |
| Ifna5 | NA | 0.00 | 0.00 |
| Ifna6 | NA | 0.00 | 0.00 |
| Ifna7 | NA | 0.00 | 0.00 |
| Ifna9 | NA | 0.00 | 0.00 |
| Ifna11 | NA | 0.00 | 0.00 |
| Ifna12 | NA | 0.00 | 0.00 |
| Ifna13 | NA | 0.00 | 0.00 |
| Ifna13 | NA | 0.00 | 0.00 |
| Ifna14 | NA | 0.00 | 0.00 |
| Ifna15 | NA | 0.00 | 0.00 |
| Ifna16 | NA | 0.00 | 0.00 |
| Ifnab | NA | 0.36 | 0.00 |
| Ifnb1 | NA | 0.00 | 0.00 |
| Ifne | NA | 0.00 | 0.00 |
| Ifng | NA | 0.00 | 0.00 |
| Ifnk | 1.18 | 7.95 | 6.72 |
| Ifnl2 | NA | 0.00 | 0.00 |
| Ifnl3 | NA | 1.10 | 0.00 |
| Ifnz | NA | 0.56 | 0.00 |
| Ifnar1 | 1.11 | 1412.08 | 1267.17 |
| Ifnar2 | 1.22 | 253.56 | 207.64 |
| Ifngr1 | -1.06 | 4043.45 | 4290.54 |
| Ifngr2 | -1.12 | 3368.70 | 3784.38 |
| Ifnlr1 | 1.22 | 513.01 | 421.71 |
| Il10rb | -1.02 | 1357.28 | 1381.12 |

**Extended Data Fig. 3 | Sca-1 is expressed in granuloma crypt epithelium and IFN-γ is present in granulomas. a**, Representative flow cytometry of Lgr5–GFP and Sca-1 in crypt cells from unfractionated duodenum preps of Lgr5–GFP mice after *H. polygyrus* infection. **b**, Flow cytometry of Sca-1 in crypt cells from biopsies from mice 6 or 10 days after infection with *H. polygyrus*. **c**, Flow cytometry of Sca-1 in crypt cells from unfractionated duodenum preps of mice 4 days after infection with *N. brasiliensis* (Nippo). **d**, Non-granuloma or granuloma biopsies from wild-type mice were analysed by qPCR for *Ifng* transcript. **e**, Fold change and read counts of IFN and IFN receptor genes from RNA-seq performed as in Extended Data Fig. 2b with no filter applied. 'NA' results from division by zero. $n = 4$ (**a**, days 2, 4, 6, **b**, day 6), 5 (**a**, day 0, **b**, day 10), 7 (**c**, controls), or 8 mice (**c**, Nippo, **d**). Statistics represent all biological replicates, and all experiments were replicated at least twice. Graphs show mean ± s.d. (**b**–**d**). $^{*}P < 0.05$, $^{**}P < 0.01$ by unpaired, two-tailed Mann–Whitney test.

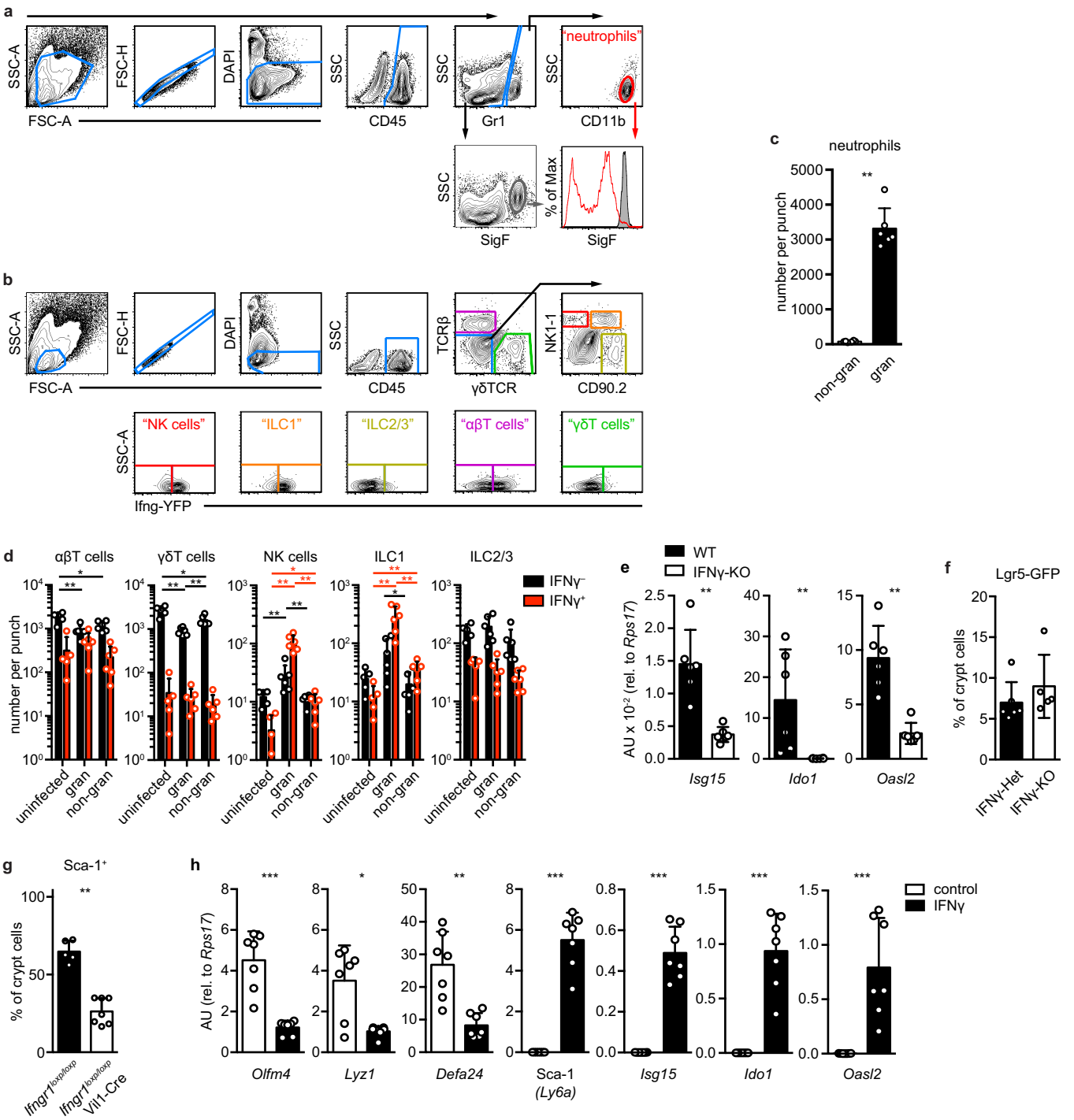


**Extended Data Fig. 4 | IFN-γ produced by *H. polygyrus*-responsive immune cells drives the granuloma gene signature. a**–**g**, Mice were infected with *H. polygyrus* and analysed at day 6, unless otherwise indicated. **a**, **b**, Representative gating example of neutrophils (**a**) and natural killer (NK) cells, ILC1, ILC2/3, αβ T cells, and γδ T cells (**b**). **c**, Neutrophils were enumerated by flow cytometry from non-granuloma (non-gran) or granuloma (gran) biopsies. **d**, *Ifng* reporter mice were untreated (uninfected) or infected (gran or non-gran) with *H. polygyrus* and analysed by flow cytometry 5–6 days later for haematopoietic (CD45$^+$) populations: NK cells, ILC1, ILC2/3, αβ T cells and γδ T cells. No reporter signal was seen in non-lymphoid populations. **e**, Crypt cells were sorted from granuloma biopsies of IFN-γ-knockout (KO) mice and analysed by qPCR for the indicated transcripts. **f**, Lgr5–GFP mice were bred with IFN-γ-knockout (KO) mice and offspring were analysed by flow cytometry for Lgr5–GFP expression in crypt epithelia from granuloma biopsies. **g**, *Ifngr1*$^{loxp/loxp}$ mice were bred with Vil1-Cre mice and analysed by flow cytometry for Sca-1 expression in crypt epithelia from granuloma biopsies. **h**, Wild type organoids were treated with 5 ng ml$^{-1}$ IFN-γ for 24 h and analysed by qPCR for the indicated transcripts. $n = 5$ mice (**d**, uninfected, **f**, KO, **g**, *Ifngr1*$^{loxp/loxp}$), 6 mice (**c**, **d**, infected, **e**, **f**, heterozygous), 7 mice (**g**, *Ifngr1*$^{loxp/loxp}$;Vil1-Cre), or 7 cultures (**h**). Statistics represent all biological replicates, and all experiments were replicated at least twice. Graphs show mean ± s.d. (**c**–**h**). $^*P < 0.05$, $^{**}P < 0.01$, $^{***}P < 0.001$ by unpaired, two-tailed Mann–Whitney test.

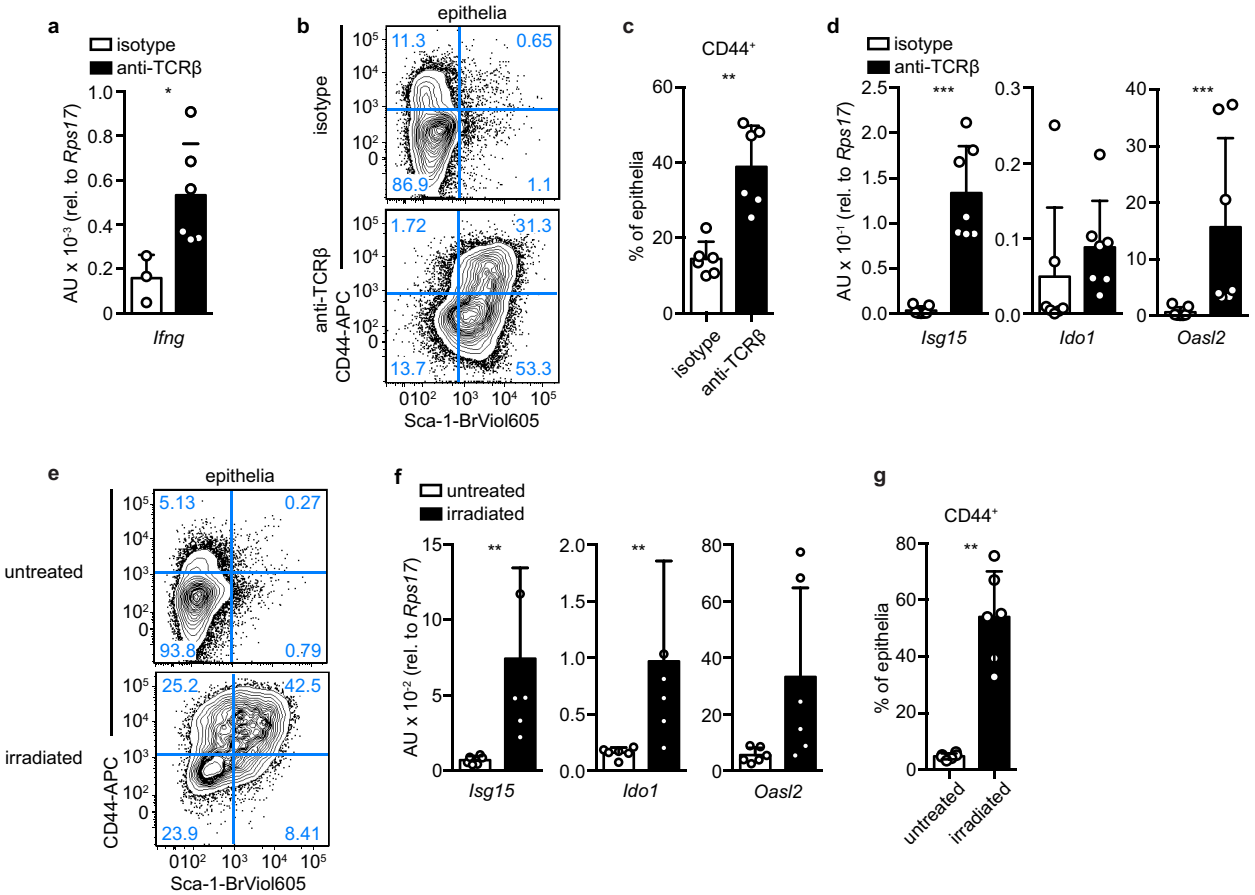


**Extended Data Fig. 5 | Inflammation via immune cell activation and irradiation induces granuloma-like epithelial responses. a–d**, Mice were treated with 20 μg isotype antibody or anti-TCRβ antibody (clone H57) and analysed 24 h later. **a**, Unfractionated tissue analysed by qPCR for *Ifng* transcript. **b**, Representative flow cytometry of CD44 and Sca-1 in total epithelium. **c**, Epithelium was assessed for crypt size by flow cytometry using frequency of CD44. **d**, Crypt cells were sorted and analysed by qPCR for the indicated transcripts. **e–g**, Mice were untreated or subjected to 10 Gy irradiation and analysed three days later. **e**, Representative flow cytometry of CD44 and Sca-1 expression on total epithelium. **f**, Crypt cells were sorted and analysed by qPCR for the indicated transcripts. **g**, Flow cytometry of the frequency of $CD44^+$ crypt cells among total epithelium. $n = 3$ (**a**, isotype), 6 (**a**, anti-TCRβ, **b**, **c**, **e–g**), or 7 mice (**d**). Statistics represent all biological replicates, and all experiments were replicated at least twice. Graphs show mean ±s.d. (**a**, **c**, **d**, **f**, **g**). $^*P < 0.05$, $^{**}P < 0.01$, $^{***}P < 0.001$ by unpaired, two-tailed Mann–Whitney test.

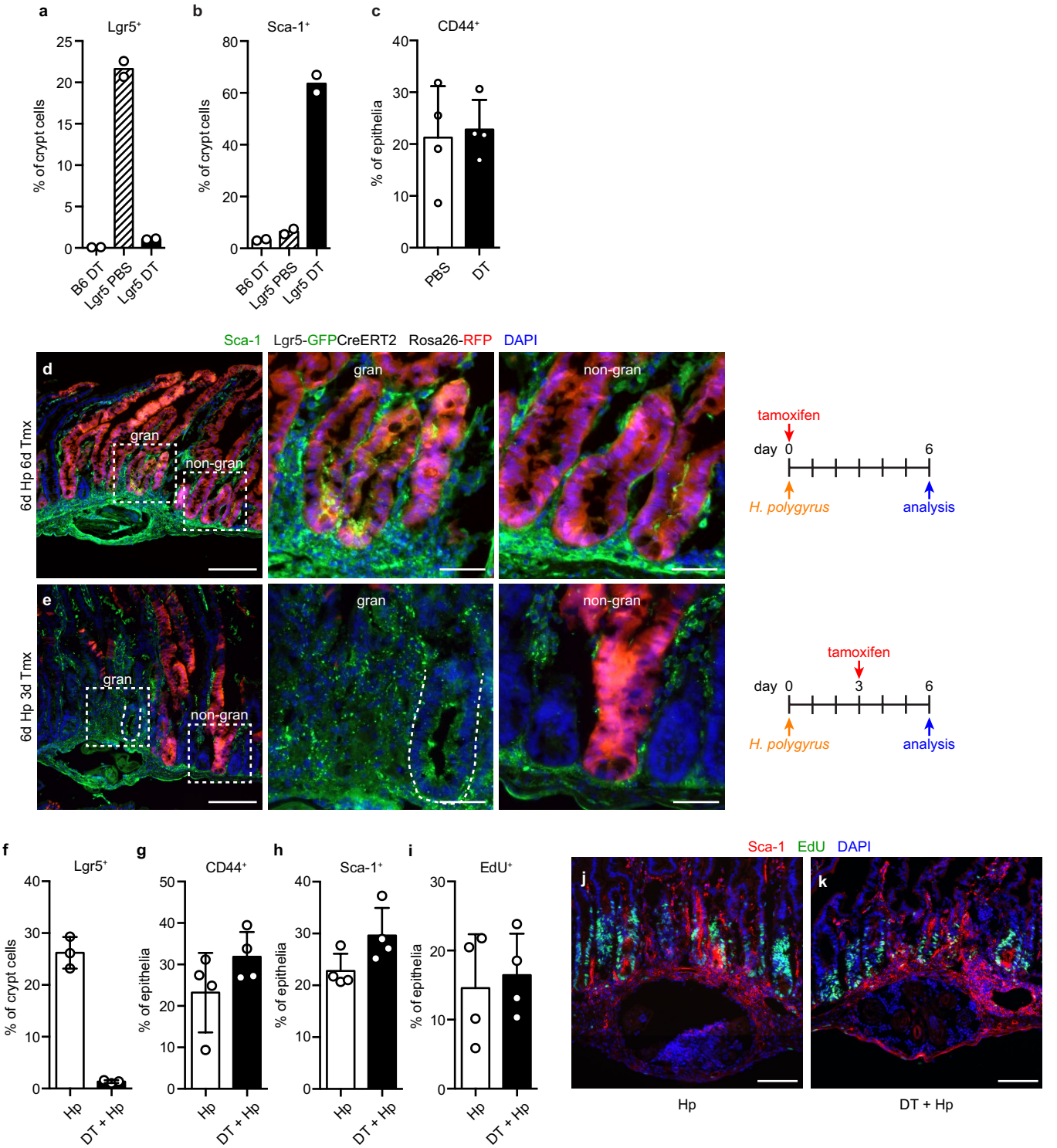


**Extended Data Fig. 6 | Granuloma crypt epithelium arises from pre-existing Lgr5$^+$ cells but does not require Lgr5$^+$ cells. a–c**, *Lgr5*$^{DTRGFP/+}$ (Lgr5) or wild-type (B6) mice were treated with diphtheria toxin (DT) and analysed a day later by flow cytometry for Lgr5–GFP (**a**), Sca-1 (**b**), or frequency of crypt cells among total epithelium (**c**). **d**, **e**, Representative images of lineage tracing of Lgr5$^+$ precursors and Sca-1 staining in crypts overlying (gran) and adjacent to (non-gran) *H. polygyrus* (Hp) granulomas. *Lgr5*$^{GFP\text{-}creERT2/+}$ *Rosa26*$^{RFP/+}$ mice were administered 2.5 mg tamoxifen (Tmx) either immediately before (**d**) or three days after (**e**) infection with *H. polygyrus*. Mice were analysed at day 6. **f–k**, *Lgr5*$^{DTRGFP/+}$ mice were treated with diphtheria toxin immediately before infection with *H. polygyrus* and analysed by flow cytometry at day 1 for Lgr5–GFP (**f**), or at day 6 for CD44 (**g**), Sca-1 (**h**) and EdU (**i**) in epithelial cells from granuloma biopsies. **j**, **k**, Representative images of Sca-1 and EdU detection at day 6. $n = 2$ (**a**, **b**, **e**), 3 (**d**, **f**, **j**, **k**), or 4 mice (**c**, **g–i**). Experiments were replicated at least twice, except the experiment in **a** and **b**, which was performed once. Graphs show mean ± s.d. (**c**, **f–i**). Scale bars: main, 200 μm; insets 50 μm (**d**, **e**), 100 μm. (**j**, **k**).

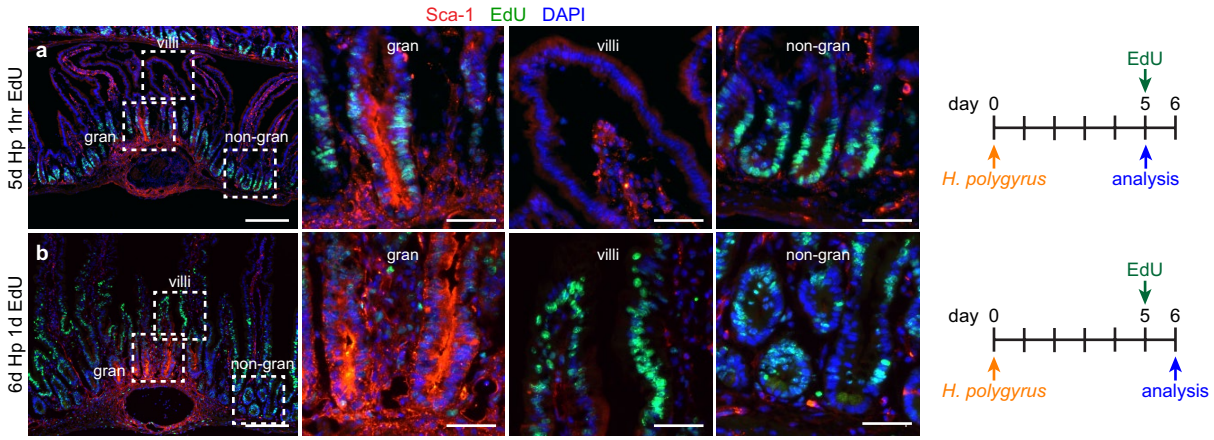


**Extended Data Fig. 7 | Granuloma crypt epithelium contributes to epithelial turnover. a**, **b**, Representative images of Sca-1 and EdU staining. Wild-type mice were injected with EdU at day 5 of infection and analysed after 1 h (**a**) or 24 h (**b**) to localize labelled cells within villi, and within crypts overlying (gran) or adjacent to (non-gran) *H. polygyrus* granulomas. $n = 4$ (**a**) or 6 mice (**b**). Experiments were replicated at least twice. Scale bars: left, 200 μm; insets, 50 μm.

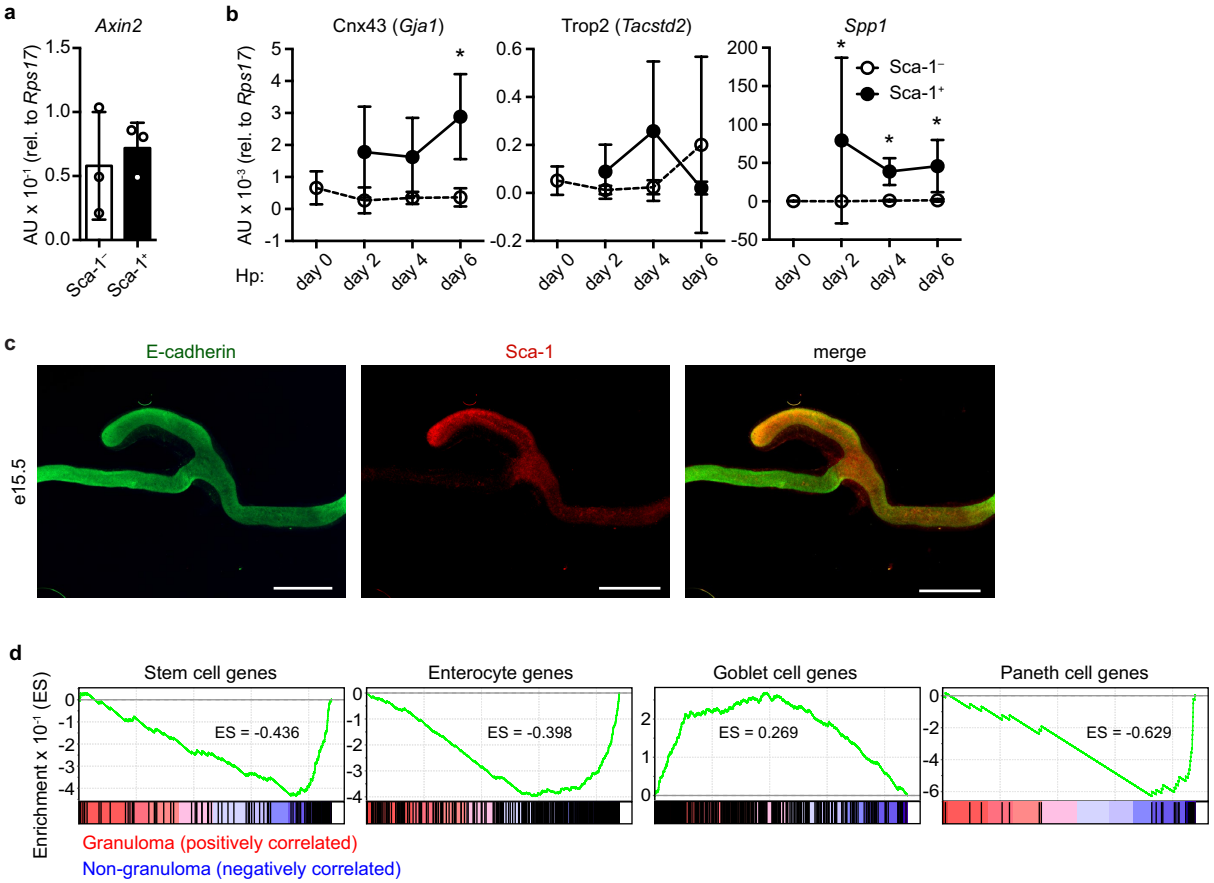


**Extended Data Fig. 8 | Granuloma crypt epithelium activates a fetal-like program and exhibits altered differentiation. a**, Material from the cultures described in Fig. 4a, b was analysed by qPCR for *Axin2* transcript. **b**, Sca-1$^+$ or Sca-1$^-$ crypt cells were sorted from mice infected with *H. polygyrus* for the indicated times and analysed by qPCR for fetal transcripts. **c**, Representative image of whole-mount e15.5 fetal intestine stained for Sca-1 and E-cadherin. **d**, Bulk RNA-seq data (as in Fig. 1e) were analysed by GSEA for intestinal epithelial signature genes[21]. Enrichment score (ES) is indicated and all analyses have FDR $<10^{-3}$. $n=3$ mice (**a**), 3 fetuses (**c**), 4 mice (**b**, day 2, 4, 6), 4 independently sorted samples (**d**, granuloma, 20 mice total), 5 mice (**b**, day 0), or 5 independently sorted samples (**d**, non-granuloma, 25 mice total). Statistics represent all biological replicates, and all experiments were replicated at least twice. Graphs show mean ± s.d. (**a**, **b**). *$P<0.05$ by unpaired, two-tailed Mann–Whitney test. Scale bar: 1 mm (**c**).

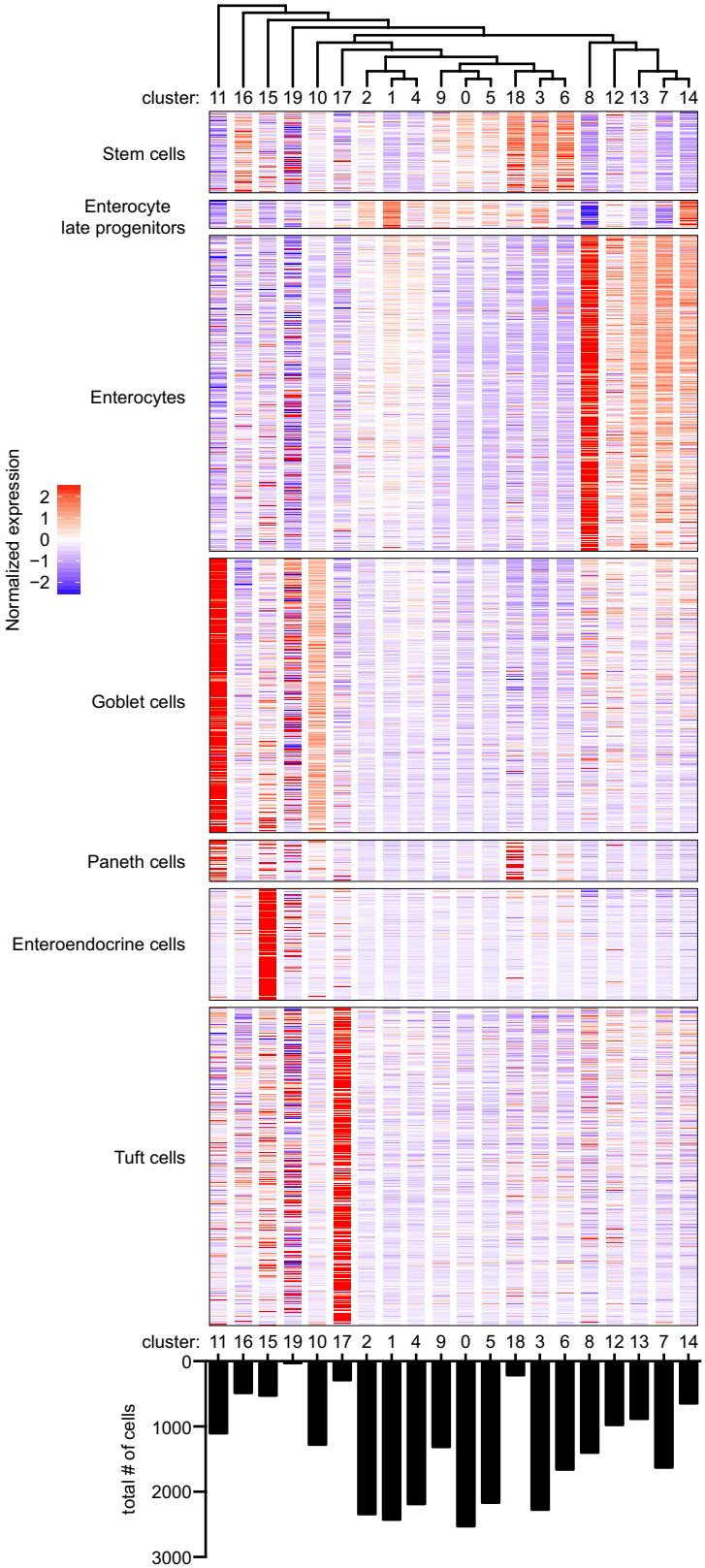


**Extended Data Fig. 9 | Markers of adult intestinal cell types in single-cell RNA-seq of Sca-1$^+$ and Sca-1$^-$ crypt epithelium.** Clusters identified by unsupervised hierarchical clustering were arranged per the unsupervised dendrogram of cluster relatedness (top) and normalized expression values for intestinal cell type gene signatures[21] were displayed as a heat map in each cluster (middle). The total number of cells in each cluster is shown (bottom).

nature research

Corresponding author(s): Richard Locksley, Ophir Klein

# Reporting Summary

Nature Research wishes to improve the reproducibility of the work that we publish. This form provides structure for consistency and transparency in reporting. For further information on Nature Research policies, see Authors & Referees and the Editorial Policy Checklist.

## Statistical parameters

When statistical analyses are reported, confirm that the following items are present in the relevant location (e.g. figure legend, table legend, main text, or Methods section).

| n/a | Confirmed | |
|---|---|---|
| ☐ | ☒ | The exact sample size (*n*) for each experimental group/condition, given as a discrete number and unit of measurement |
| ☐ | ☒ | An indication of whether measurements were taken from distinct samples or whether the same sample was measured repeatedly |
| ☐ | ☒ | The statistical test(s) used AND whether they are one- or two-sided<br>*Only common tests should be described solely by name; describe more complex techniques in the Methods section.* |
| ☒ | ☐ | A description of all covariates tested |
| ☐ | ☒ | A description of any assumptions or corrections, such as tests of normality and adjustment for multiple comparisons |
| ☐ | ☒ | A full description of the statistics including central tendency (e.g. means) or other basic estimates (e.g. regression coefficient) AND variation (e.g. standard deviation) or associated estimates of uncertainty (e.g. confidence intervals) |
| ☒ | ☐ | For null hypothesis testing, the test statistic (e.g. *F*, *t*, *r*) with confidence intervals, effect sizes, degrees of freedom and *P* value noted<br>*Give P values as exact values whenever suitable.* |
| ☒ | ☐ | For Bayesian analysis, information on the choice of priors and Markov chain Monte Carlo settings |
| ☒ | ☐ | For hierarchical and complex designs, identification of the appropriate level for tests and full reporting of outcomes |
| ☒ | ☐ | Estimates of effect sizes (e.g. Cohen's *d*, Pearson's *r*), indicating how they were calculated |
| ☐ | ☒ | Clearly defined error bars<br>*State explicitly what error bars represent (e.g. SD, SE, CI)* |

*Our web collection on statistics for biologists may be useful.*

## Software and code

Policy information about availability of computer code

| | |
|---|---|
| Data collection | FACSDiva v8.0.1; Summit v5.2; ImageJ v1.48; AxioVision v4.8.2; Leica Applications Suite v4.9; QuantStudio v1.2; StepOne v2.1 |
| Data analysis | FlowJo v9.9; Prism v6.0h; Excel v14.7.7; Photoshop CS6; Seurat v2.0; STAR v.2.4.0j; CellRanger v2.1; GeneProf (2017); GSEA v3.0; Ingenuity Pathway Analysis (Summer Release 2015); Morpheus (https://software.broadinstitute.org/morpheus); Interferome (http://www.interferome.org) |

For manuscripts utilizing custom algorithms or software that are central to the research but not yet described in published literature, software must be made available to editors/reviewers upon request. We strongly encourage code deposition in a community repository (e.g. GitHub). See the Nature Research guidelines for submitting code & software for further information.

## Data

Policy information about availability of data

All manuscripts must include a data availability statement. This statement should provide the following information, where applicable:

- Accession codes, unique identifiers, or web links for publicly available datasets
- A list of figures that have associated raw data
- A description of any restrictions on data availability

The RNA sequencing data reported in this study are available at the Gene Expression Omnibus under accession codes GSE97405 (bulk) and GSE108233 (single-cell).

# Field-specific reporting

Please select the best fit for your research. If you are not sure, read the appropriate sections before making your selection.

☒ Life sciences ☐ Behavioural & social sciences

For a reference copy of the document with all sections, see nature.com/authors/policies/ReportingSummary-flat.pdf

# Life sciences

## Study design

All studies must disclose on these points even when the disclosure is negative.

| | |
|---|---|
| Sample size | In most cases we assumed a minimum of 4 mice would be required to recognize differences between genotypes or conditions, based upon historical experiments in other contexts. A minimum number of animals were used to conform with NIH guidelines. |
| Data exclusions | For the bulk RNA sequencing experiment, two granuloma data sets were excluded due to low unique mapping rates and failure to group by tissue in principle components analysis and hierarchical clustering. |
| Replication | All experiments were replicated at least twice with similar findings, except single cell RNAseq due to prohibitive cost. We also did not replicate Diphtheria Toxin treatment of wild type mice for Sca-1 induction (Extended Data Figure 6a,b) due to clear and expected results for this reviewer requested control. These are noted in the text under "Statistics". |
| Randomization | Samples were randomly assigned. |
| Blinding | Investigators were not blinded to group allocation because treatments and data collection were performed by the same people. |

## Materials & experimental systems

Policy information about availability of materials

| n/a | Involved in the study |
|---|---|
| ☐ | ☒ Unique materials |
| ☐ | ☒ Antibodies |
| ☒ | ☐ Eukaryotic cell lines |
| ☐ | ☒ Research animals |
| ☒ | ☐ Human research participants |

### Unique materials

| | |
|---|---|
| Obtaining unique materials | Lgr5(DTRGFP) mice can be used with permission from Genentech. |

### Antibodies

| | |
|---|---|
| Antibodies used | CD45 (Biolegend #103106, Clone 30-F11, various lot #s) CD326/EpCAM (Biolegend #118210, Clone G8.8, various lot #s) CD44 (Biolegend #103018, Clone IM7, various lot #s) Sca-1 (Biolegend #108134, Clone D7, various lot #s) TCRβ (Biolegend #109218, Clone H57, various lot #s) γδTCR (Biolegend #109218, Clone GL3, various lot #s) NK1.1 (Biolegend #108728, Clone PK136, various lot #s) CD90.2 (Biolegend #140318, Clone 53-2.1, various lot #s) CD11b (Biolegend #301332 Clone M1/70, various lot #s) Gr1 (Biolegend # 108428, Clone RB6-8C5, various lot #s) GFP (Aves #GFP-1020, Clone NA (Polyclonal), Lot# GFP697986) GFP (Abcam #ab13790, Clone NA (Polyclonal), Lot# GR236651-8)Ki67 (Thermo# RM-9106, Clone Sp6, various lot #s) E-Cadherin (Cell Signaling Technology #3195, Clone 24E10, Lot# 13) Sca-1 (Biolegend #122502, Clone e13-161.7, Lot# B186579) Muc2 (Santa Cruz #SC-15334, Clone NA (Polyclonal), various lot #s, no longer available) MMP7 (R&D Systems #AF2967, Clone NA (Polyclonal), Lot #YLS0214071) |
| Validation | Validation statements available from manufacturers: GFP, (Aves #GFP-1020, http://www.aveslab.com/wp-content/uploads/GFP-10201.pdf) GFP (Abcam #ab13790, http://www.abcam.com/gfp-antibody-ab13970.html) Ki67 (Thermo #RM-910, https://www.thermofisher.com/order/catalog/product/RM-9106-R7 ) E-Cadherin (Cell Signaling Technology #3195, https://www.cellsignal.com/products/primary-antibodies/e-cadherin-24e10-rabbit-mab/3195) Sca-1 (Biolegend #122502, https://www.biolegend.com/en-us/products/purified-anti-mouse-ly-6a-e-sca-1-antibody-3892) Muc2 (Santa Cruz #SC-15334, No longer available from Santa Cruz) MMP7 (RD #AF2967, https://resources.rndsystems.com/pdfs/datasheets/af2967.pdf) CD11b (BioLegend #301332, https://www.biolegend.com/en-us/products/brilliant-violet-605-anti-human-cd11b-antibody-8493) CD326/EpCAM (BioLegend #118210, https://www.biolegend.com/en-us/products/alexa-fluor-488-anti-mouse-cd326-ep-cam-antibody-4972) CD44 (BioLegend #103018, https://www.biolegend.com/en-us/products/alexa-fluor-647-anti-mouse-human-cd44-antibody-3098) CD45 (BioLegend 103106, https://www.biolegend.com/en-us/products/pe-anti-mouse-cd45-antibody-100) CD90.2 (BioLegend #140318, https://www.biolegend.com/en-us/products/brilliant-violet-605-anti-mouse-cd90-2-thy-1-2- |

antibody-7866)
Gr1 (BioLegend #108428, https://www.biolegend.com/en-us/products/percp-cy5-5-anti-mouse-ly-6g-ly-6c-gr-1-antibody-4286)
NK1.1 (BioLegend #108728, https://www.biolegend.com/en-us/products/percp-cy5-5-anti-mouse-nk-1-1-antibody-4289)
Sca-1 (BioLegend, #108134, https://www.biolegend.com/en-us/products/brilliant-violet-605-anti-mouse-ly-6a-e-sca-1-antibody-8664)
TCRβ (BioLegend, #109218, https://www.biolegend.com/en-us/products/alexa-fluor-647-anti-mouse-tcr-beta-chain-antibody-3272)
γδTCR (BioLegend #118108, https://www.biolegend.com/en-us/products/pe-anti-mouse-tcr-gamma-delta-antibody-2421)

### Research animals

Policy information about studies involving animals; ARRIVE guidelines recommended for reporting animal research

| | |
|---|---|
| Animals/animal-derived materials | Male and female mice aged 6–14 weeks, weighing 20-30 grams, were used for all experiments, except those analyzing fetal tissue. Lgr5DTRGFP mice were from Genentech. Wild-type (C57BL/6J), Lgr5GFP-CreERT2/+ (B6.129P2-Lgr5tm1(cre/ERT2)Cle/J), Rosa26RFP/+ (B6;129S6-Gt(ROSA)26Sortm14(CAG-tdTomato)Hze/J), IFNγ reporter (B6.129S4-Ifngtm3.1Lky/J), IFNγ-null (B6.129S7-Ifngtm1Ts/J), IFNγ receptor-flox (Ifngr1loxP/loxP; C57BL/6N-Ifngr1tm1.1Rds/J), and Vil1-Cre (B6.Cg-Tg(Vil1-cre)997Gum/J) mice were from The Jackson Laboratory (Bar Harbor, Maine). |

# Method-specific reporting

| n/a | Involved in the study |
|---|---|
| ☒ | ☐ ChIP-seq |
| ☐ | ☒ Flow cytometry |
| ☒ | ☐ Magnetic resonance imaging |

## Flow Cytometry

### Plots

Confirm that:

☒ The axis labels state the marker and fluorochrome used (e.g. CD4-FITC).

☒ The axis scales are clearly visible. Include numbers along axes only for bottom left plot of group (a 'group' is an analysis of identical markers).

☒ All plots are contour plots with outliers or pseudocolor plots.

☒ A numerical value for number of cells or percentage (with statistics) is provided.

### Methodology

| | |
|---|---|
| Sample preparation | The duodenum was dissected, flushed extensively with cold PBS, and the mesenteric tissue was removed. For whole tissue preps, Peyer's patches were removed and tissue was turned inside-out. For recovery of punch biopsies tissue was fileted open longitudinally. In both cases, tissue was shaken in three changes of 20 ml cold PBS and washed for 20 minutes at 37°C in two changes of 20 ml Ca2+/Mg2+-free HBSS containing 5 mM DTT, 10 mM HEPES, and 2% FCS, followed by 20 ml of Ca2+/Mg2+-replete HBSS containing 10 mM HEPES and 2% FCS. For punch biopsies, granuloma and non-granuloma tissue was dissected with a 1 mm punch tool under low-power magnification. Tissues were digested for 30 minutes at 37°C in 5 ml (whole tissue) or 2 ml (punch biopsies) Ca2+/Mg2+-replete HBSS containing 10 mM HEPES, 2% FCS, 30 µg/ml DNaseI (Roche), and 0.1 Wünsch/ml LibTM (Roche), and whole tissue was homogenized in C tubes using a gentleMACS tissue dissociator (Miltenyi). Homogenate or punch biopsies were passed through a 100 µm filter with assistance of a 3 ml syringe plunger, and enumerated for staining equivalent numbers for flow cytometry or sorting. Fc Block (anti-CD16/32), doublet exclusion, and DAPI exclusion were used in all cases. |
| Instrument | Becton Dickinson Fortessa; Beckman Coulter MoFlo XDP |
| Software | FACSDiva v8.0.1; FlowJo v9.9; Summit v5.2 |
| Cell population abundance | In all cases, sorted cells were checked for purity by running a fraction of the sorted material on a cytomtery, including fresh DAPI to exclude dead cells. Prior to determination of purity, events were gated for FSC x SSC to exclude bubbles and debris in the sample collection tube, and only DAPI(lo) events were considered. Sorted samples generally had a purity >90%. Samples that were obviously outliers for the frequency of DAPI+ events or of obviously low purity were removed from downstream analysis, on a case-by-case basis. |
| Gating strategy | For gating of intestinal epithelial populations, data were generally gated in a linear fashion as follows: 1) time x FSC to exclude events influenced by initial sampling by the cytometer and by exhaustion of the sample, 2) FSC x SSC chosen to includes epithelial cells, 3) FSC-height x FSC-area to exclude doublets, 4) DAPI x FSC to exclude DAPI+ events, 5) CD45 x SSC to exclude CD45+ events, 6) CD326 x CD44 to include CD326+ events, 7) CD326 x CD44 to include CD326+ CD44+ events, 8a) Sca-1 x Lgr5, and/or 8b) Sca-1 x SSC, and/or 8c) Lgr5 x SSC. See Extended Data Figure 2a.<br><br>For gating of intestinal neutrophils, data were generally gated in a linear fashion as follows: 1) time x FSC to exclude events influenced by initial sampling by the cytometer and by exhaustion of the sample, 2) FSC x SSC chosen to includes epithelial cells, |

3) FSC-height x FSC-area to exclude doublets, 4) DAPI x FSC to exclude DAPI+ events, 5) CD45 x SSC to include CD45+ events, 6) Gr1 x SSC to included Gr1+ events, 7) CD11b x SSC. See Extended Data Figure 4a.

For gating of intestinal lymphoid populations, data were generally gated in a linear fashion as follows: 1) time x FSC to exclude events influenced by initial sampling by the cytometer and by exhaustion of the sample, 2) FSC x SSC chosen to includes epithelial cells, 3) FSC-height x FSC-area to exclude doublets, 4) DAPI x FSC to exclude DAPI+ events, 5) CD45 x SSC to include CD45+ events, 6) TCRb x gdTCR to gate abT cells, gdT cells, and non-T cells, 7) of non-T cells, NK1.1 x CD90.2, 8) Great x SSC. See Extended Data Figure 4b.

☒ Tick this box to confirm that a figure exemplifying the gating strategy is provided in the Supplementary Information.